Sequential action of *jnk* genes establishes the embryonic left-right axis

Christopher J. Derrick*, Adrian Santos-Ledo*, Lorraine Eley, Deborah J. Henderson and Bill Chaudhry‡

Biosciences Institute, Faculty of Medical Sciences, Newcastle University, International Centre for Life, Central Parkway, Newcastle upon Tyne, NE1 3BZ.

*equal contribution

‡Corresponding Author: Dr Bill Chaudhry

Biosciences Institute, Faculty of Medical Sciences, Newcastle University,

International Centre for Life, Central Parkway

Newcastle upon Tyne, NE1 3BZ

bill.chaudhry@ncl.ac.uk

Tel: +44(0)191 241 8681

Key words: jnk, laterality, PCP, zebrafish, Kupffer's Vesicle, cilia

Summary Statement

This study identifies that different members of the *JNK* gene family play sequential roles in establishing the left-right axis through early regulation of motile cilia and later restriction of *pitx2c* expression.

Abstract

The establishment of the left-right axis is critical for the placement, morphogenesis and function of internal organs. Left-right specification is proposed to be dependent on cilia-driven fluid flow in the embryonic node. Planar cell polarity (PCP) signalling is critical for patterning of nodal cilia, yet downstream effectors driving this process remain elusive. We have examined the role of the *JNK* gene family, a proposed downstream component of PCP signalling, in the development and function of the zebrafish node. We show *jnk1* and *jnk2* specify length of nodal cilia, generate flow in the node and restrict *Nodal* to the left lateral

plate mesoderm. Moreover, loss of asymmetric *Nodal* expression does not result in disturbances to asymmetric organ placement, supporting a model that nodal flow may be dispensable for organ laterality. Later, *jnk3* is required to restrict *pitx2c* expression to the left side and permit correct endodermal organ placement. This work uncovers multiple roles for the *JNK* gene family acting at different points during left-right axis establishment. It highlights extensive redundancy and indicates JNK activity is distinct from the PCP signalling pathway.

INTRODUCTION

Vertebrates exhibit external symmetry, however, many internal organs have asymmetric positioning requiring establishment of a midline left-right axis in early development (Blum and Ott, 2018; Grimes and Burdine, 2017). Disruption to this axis can result in abnormal organ positioning and when associated with congenital heart malformations, is known as heterotaxy (Kennedy et al., 2007; Shiraishi and Ichikawa, 2012). The embryonic node, a transient, ciliated cavity or pit is believed to be essential for the establishment of left-right identity. Within the node, rotation of nodal cilia generate right-to-left fluid flow (nodal flow) (Amack, 2014; Nonaka et al., 1998), leading to asymmetric expression of the TGF-β family member *Nodal* in the left lateral plate mesoderm (LPM) (Tabin, 2005). *Nodal* expression is self-promoting (Yamamoto et al., 2003) and concomitantly activates its own inhibitors, in particular *Lefty1* in the midline, which prevents Nodal signalling propagating into the right LPM (Meno et al., 1998; Nakamura et al., 2006). Downstream of *Nodal*, the highly conserved transcription factor *Pitx2* (Shiratori et al., 2001) is expressed in the left LPM overlapping multiple organ analgen that undergo asymmetric morphogenesis (Campione et al., 1999). The *Pitx2* gene locus generates two distinct mRNAs, *Pitx2a* and *Pitx2c* that perform subtly different roles in development (Essner et al., 2000). Left-right axis establishment is well conserved in zebrafish, where function of the node, or Kupffer's Vesicle (KV) (Essner et al., 2005; Kupffer, C, 1868), is proposed to promote left-sided expression of the *Nodal* homolog *southpaw* (*spaw*) (Long et al., 2003). Zebrafish abdominal organs are asymmetrically positioned, with left-sided positioning of the liver and right-sided positioning of the stomach, pancreas and spleen (Horne-Badovinac et al., 2003). In the heart, the first evidence of morphological left-right identity is manifested as jogging, the extension of the linear heart tube under the left eye (Chen et al., 1997; Smith and Uribe, 2021). Dextral heart looping establishes the asymmetric placement of the single atrium and ventricle.

Within the node, motile cilia are positioned distally on each cell (Nonaka et al., 2005), a patterning governed by the highly conserved Wnt planar cell polarity (PCP) pathway (Hashimoto et al., 2010; Minegishi et al., 2017). This pathway also plays critical roles in regulating polarised cellular behaviours that drive convergent-extension movements during gastrulation (Roszko et al., 2009). Thus, mutations in classical PCP components result in a striking convergent-extension phenotype, seen in zebrafish as shortening of the antero-posterior axis (Jessen et al., 2002; Park and Moon, 2002). Loss of key components of the PCP pathway also impact node development. Vangl2 plays a role in defining the size of the node and positioning nodal cilia, whilst *rock2b* establishes their asymmetric antero-posterior arrangement (Borovina et al., 2010; Wang et al., 2011). A proposed downstream effector of PCP signalling is the highly conserved c-Jun N-terminal Kinase (JNK), (Boutros et al., 1998; Moriguchi et al., 1999; Riesgo-Escovar et al., 1996), Ser/Thr kinases that are members of the Mitogen Activated Protein Kinase (MAPK) superfamily activated through a MAPKKK, MAPKK, MAPK phosphorylation cascade (Davis, 2000). Vertebrates have three *JNK* genes: *JNK1*, *JNK2* and *JNK3* (Gupta et al., 1996), *JNK1* and *JNK2* are ubiquitously expressed whilst *JNK3* expression is restricted to specific structures (Davis, 2000; Santos-Ledo et al., 2020). Double *Jnk1/Jnk2* knockout mouse mutants are embryonic lethal between Embryonic Day (E)11 and E12, whilst *Jnk1/Jnk3* or *Jnk2/Jnk3* double mutants are reported to be healthy, demonstrating redundancy and suggesting that genetic compensation could be active in the *JNK* gene family, but also questions a direct role for JNK in the PCP pathway (Kuan et al., 1999). Similarly, our recent studies using zebrafish mutants do not implicate the duplicated *jnk1a* and *jnk1b* genes in either the PCP pathway or left-right axis specification (Santos-Ledo et al., 2020). In contrast, other studies using anti-sense morpholino oligonucleotides have proposed that *jnk1* is required for specifying left-right axis through correct nodal cilia length and suggested *jnk1* morphants display defects in heart jogging. More generally, shorter nodal cilia are widely reported to impact on left-right asymmetry (Gao et al., 2017; Heigwer et al., 2020; Jacinto et al., 2021; Lopes et al., 2010; Neugebauer et al., 2009; Schottenfeld et al., 2007; Yamauchi et al., 2009). Separately, experiments in *Xenopus* have suggested a cooperative role for JNK in the PCP pathway (Kim and Han, 2005; Yamanaka et al., 2002)

Using zebrafish to investigate the link between node function and organ asymmetry (Smith and Uribe, 2021), we set out to address whether a role exists for members of the *jnk* family in regulating left-right axis development and whether genetic compensation between *jnk* family members may obscure PCP functions. Generating stable mutants, we characterised the impact of loss of the four zebrafish *jnk* genes on nodal cilia development and the

subsequent result on organ asymmetry. We identify that *jnk1a, jnk1b* and *jnk2* function non-redundantly in the embryonic node to specify nodal cilia length and are required for directional nodal flow. We show that compromised KV function following loss of *jnk1a*, *jnk1b* and *jnk2*, although impacting disrupting lateralised expression of *spaw,* does not result in abnormal organ asymmetry, defining an early, yet dispensable role for *jnk1* and *jnk2* in left-right axis establishment. We also identify a novel, later requirement for *jnk3* in restricting *pitx2c* expression and promoting lateralised endodermal organ placement.

RESULTS

We have previously reported that *Maternal Zygotic jnk1a (MZjnk1a)*, *MZjnk1b* and *MZjnk1a*;*MZjnk1b* zebrafish mutants display no evidence of left-right disturbance with regard to heart development (Santos-Ledo et al., 2020). However, a morpholino-based study suggested a role for *jnk1* in regulating nodal cilia length (Gao et al., 2017). Therefore, we set out to characterise the impact of loss of *jnk* on left-right axis development in zebrafish.

jnk1a and *jnk1b* specify length of nodal cilia and are required for nodal flow in KV

We firstly examined the impact of loss of *jnk1* activity on KV size using wholemount mRNA *in situ* hybridisation (WISH) for *dand5* (*DAN domain family member 5,* formerly *charon*) at 8 somite stage (ss) (Fig. S1A), showing comparable KV size between wild-type (WT), *MZjnk1a*, *MZjnk1b* and *MZjnk1a;MZjnk1b* mutants (Fig. S1B). We next characterised number, distribution and length of cilia within KV at 10ss using immunohistochemistry (Fig. 1A-E). Whilst total cilia number and antero-posterior distribution was unaffected in any *MZjnk1* null mutants (Fig. 1F,G), both *MZjnk1a* and *MZjnk1b* mutants displayed a subtle decrease in the length of nodal cilia (2.6% and 3.1% respectively) (Fig. 1H). However, in *MZjnk1a*;*MZjnk1b* double mutants there was a 17.6% reduction in cilia length, demonstrating redundancy of these *jnk1* paralogues in regulating KV cilial length (Fig. 1H). Surprisingly, despite relatively minor reduction in cilial length, there were significant reductions in the counter clockwise nodal flow in both *MZjnk1a* and *MZjnk1b* mutant embryos (Fig. 2C,D,F, Movies 1-3), and a greater reduction in KV flow in *MZjnk1a*;*MZjnk1b* mutants (Fig. 2E,F, Movie 4), potentially indicating reduction in cilia motility as well as length.

Normal organ positioning despite disturbed *southpaw* expression in *jnk1* mutants

Leftward flow within KV is proposed to drive left-sided expression of *southpaw* (*spaw*) (Long et al., 2003; Yamamoto et al., 2003). We therefore examined *spaw* expression at 12-14ss in our *MZjnk1* mutants (Fig. 3A-B) to determine the effect of altered nodal flow. Despite marked reduction in KV flow (Fig. 2F), there was no significant increase in isolated right-sided *spaw* expression (Fig. 3B) but there were increases in penetrance of bilateral *spaw* expression in *MZjnk1b* and *MZjnk1a*;*MZjnk1b* mutants, suggesting that loss of *jnk1b* disrupts KV function (Fig. 3B). We then investigated if abnormal *spaw* expression would translate into abnormal organ positioning. Left-sided expression of *spaw* is required for leftward heart jogging, at 1dpf (day post-fertilisation) (Lenhart et al., 2013; Noël et al., 2013; Smith et al., 2008; Veerkamp et al., 2013) (Fig. 3C) and the asymmetric movements of the LPM, positioning the liver on the left and the pancreas on the right of the midline (Horne-Badovinac et al., 2003; Yin et al., 2010) (Fig. 3E). In keeping with correct lateralised *spaw* expression, heart jogging and liver/pancreas positioning was normal in *MZjnk1a* mutants (Fig. 3D,F). However, despite the increase in bilateral *spaw* expression in *MZjnk1b* and *MZjnk1a*;*MZjnk1b* mutants (Fig. 3B), there was no disturbance of heart jogging or abdominal organ placement (Fig. 3D,F). To investigate the uncoupling between *spaw* laterality and organ asymmetry in *jnk1* mutants we examined the expression of the highly conserved Nodal-target gene *paired-liked homeodomain 2,* (*pitx2*) in the LPM at 18-19ss (Fig. 3G). Although we observed predominantly left-sided expression of the *pitx2c* spliceoform in WT, we were surprised to see high frequencies of absent and bilateral expression (Fig. 3H). Expression of *pitx2c* in *MZjnk1a*, *MZjnk1b* and *MZjnk1a*;*MZjnk1b* was comparable to WT controls and no increase in bilateral *pitx2c* expression was observed (Fig. 3H).

Taken together, these data show that *jnk1* is required for the specification of cilial length, nodal flow in KV and lateralised *spaw* expression. However, bilateral *spaw* expression in *jnk1* mutants does not translate into bilateral *pitx2c* expression, nor abnormal organ placement, suggesting other factors acting parallel to the KV axis could be functioning to drive asymmetric organ positioning or that other genes function redundantly with *jnk1* to establish laterality.

jnk2 acts with *jnk1a* and *jnk1b* to regulate early left-right axis development

Members of the *JNK* family, particularly *JNK1* and *JNK2* have been suggested to compensate for one another, (Kuan et al., 1999) we therefore generated *jnk2* mutants using CRISPR-Cas9 genome editing to investigate if compensation was occurring within KV (Fig.

S2A-B). As with *MZjnk1* mutants, *MZjnk2* mutants were fertile and appear morphologically normal (Fig. 4A). We first characterised the impact of loss of *jnk2* on KV structure and function, noting a small increase in KV size associated with increased number of nodal cilia (Fig. S2C, Fig 4C). Although normally distributed across the KV (Fig. S2D), *MZjnk2* mutants had significantly shorter nodal cilia (17.3%) (Fig. 4D); similar to *MZjnk1a*;*MZjnk1b* mutants (Fig. 1H). Whilst *MZjnk2* mutants maintain a counter-clockwise nodal flow that is reduced (Fig. 4E-E', Movie 5) this was small and not in keeping with dramatic changes seen in the *MZjnk1* mutants, suggesting cilial motility might be additionally impaired in the *MZjnk1* mutants. Confirming a minimal impact on KV function, *spaw* expression was normal (Fig. 4F), but surprisingly, there was a significant increase in the proportion of *MZjnk2* embryos without *pitx2c* expression in the LPM (Fig. 4G), however despite this, heart and abdominal organ placement was normal (Fig. 4H-I).

Having identified a partially overlapping role for *jnk2* with *jnk1a* and *jnk1b* in KV, we generated *MZjnk1a;MZjnk1b;Zjnk2 (Z, zygotic)* mutants to examine potential redundancy between *jnk1* and *jnk2*. *MZjnk1a;MZjnk1b;Zjnk2* mutants did not display any overt morphological abnormalities, KV size was normal, as was number and distribution of cilia (Fig. 5A-E). However, there was a 47% reduction in nodal cilial length and a 59% reduction in speed of nodal flow (Fig. 5F-G') in which injected beads showed no directional movement, demonstrating a loss of KV function (Movie 6). The expression pattern of *spaw* was greatly disturbed in *MZjnk1a;MZjnk1b;Zjnk2* mutants, with 40% exhibiting either right-sided or bilateral expression (Fig. 6A). Despite these severe disturbances there was no increase in the proportion of embryos which displayed bilateral or right-sided *pitx2c* expression, but instead there was an increase in the proportion of *MZjnk1a;MZjnk1b;Zjnk2* mutants without *pitx2c* expression in the LPM (Fig. 6B).

Having established that loss of *jnk1* and *jnk2* has a dramatic impact on KV function resulting in disrupted *spaw* expression, we characterised the result of these early defects on organ asymmetry at 72hpf. Using a combination of *myosin, light chain 7, regulatory* (*myl7)* and *forkhead box A3 (foxa3)* anti-sense mRNA probes for WISH, we examined the directionality of heart (Fig. 6C-C'') and gut looping (Fig. 3E-E'') in the same embryo. We did not observe any differences in organ asymmetry in *MZjnk1a*;*MZjnk1b*;*Zjnk2* mutants compared to their siblings (heterozygotes or wildtype for the *jnk2* mutation) or a WT population (Fig. 6D-E). In summary, significant disruption to the lateralised expression of *spaw* and *pitx2c* in *MZjnk1a;MZjnk1b;Zjnk2* mutants does not translate to loss of stereotypical asymmetric

organ placement. This suggests that other mechanisms, functioning in parallel to nodal flow, can correctly establish organ asymmetry during early development.

jnk3 functions distinctly from other *jnk* family members in generation of left-right asymmetry

To complete our analysis, we also generated *jnk3* mutants by CRISPR-Cas9 mutagenesis (Fig. S3A,B). As with all our generated *jnk* mutants, *MZjnk3* mutants are morphologically normal and fertile (Fig. 7A). Similar to *MZjnk2* mutants, there was an increase in the number of nodal cilia present in KV of *MZjnk3* mutants, but KV size was unaffected (Fig. 7C, Fig S3C). Cilia length and distribution was normal in *MZjnk3* mutants (Fig. 7D, Fig. S3D). Despite normal cilia length, there was a 25% reduction in speed of nodal flow but similar to other single *jnk* mutants, directionality was not affected (Fig. 7E-E', Movie 7), and the function of KV was sufficient to ensure normal expression of *spaw* in the LPM (Fig. 7F). Strikingly, and in contrast to normal *spaw* expression, 25% of *MZjnk3* mutants demonstrated bilateral *pitx2c* expression (Fig. 7G). This did not impact on heart jogging (Fig. 7H), but did correlate with the abnormal presence of bilateral liver and pancreatic anlagen in 20% of *MZjnk3* embryos (Fig. 7I).

We next generated *MZjnk1a;MZjnk1b;Zjnk3* mutants (Fig. S4A) to further examine potential compensation in the *jnk* gene family. Loss of zygotic *jnk3* had no impact on the severity of the *MZjnk1a*;*MZjnk1b* phenotype with respect to cilia length or distribution and the reduction in KV flow was comparable to *MZjnk1a;MZjnk1b* mutants (Fig. S4B-F', Movie 8). These findings suggest that *jnk3* may act downstream of *jnk1* in an epistatic mechanism. We also characterised organ looping in *MZjnk1a;MZjnk1b;Zjnk3* mutants and did not observe any significant disturbances to laterality (Fig. S4G-H).

Having established that all *jnk* genes play a role in generating nodal flow, but to seemingly different extents, we analysed flow patterns within anterior and posterior compartments of KV (Fig. S5). This identified that the main contributing factor to a reduction in flow is disruption to flow the anterior compartment of KV (Fig. S5A) whilst posterior flow was only significantly affected when both *jnk1a* and *jnk1b* were absent (Fig S5B). This analysis also confirmed that *MZjnk1a;MZjnk1b;Zjnk2* mutants display the most compromised KV function, particularly in the anterior compartment (Fig. S5A).

Although we wished to examine KV structure and function in *MZjnk1a;MZjnk1b;Zjnk2;Zjnk3* mutant embryos, this proved difficult as both *jnk2* and *jnk3* lie on chromosome 21 and breeding between these alleles could only produce heterozygotes in *trans*. Meiotic recombination events that would bring *jnk2* and *jnk3* alleles into *cis* were extremely rare (<1%) and we were not successful in establishing the line.

jnk1 and *jnk2* are required to establish the midline barrier

Analysis of left-right specification in *jnk* mutants identified that bilateral expression of *spaw* is the principal abnormality seen in *MZjnk1a;MZjnk1b;Zjnk2* mutants (Fig. 6A), whereas bilateral *pitx2c* expression is observed in *MZjnk3* mutants (Fig. 7H). This suggests that the midline barrier might be dependent on *jnk* activity. In WT at 13-14ss, *lefty1* (*lft1)* expression extends anteriorly from the caudal region of the embryo, setting up a molecular barrier to maintain left-sided *spaw* expression. (Fig. 8A,B). We identified a failure in the propagation of *lft1* in *MZjnk1a*, *MZjnk1b* and *MZjnk1a*;*MZjnk1b*, null embryos (Fig. 8C-E,I), with a less severe reduction in the length of the *lft1* domain in *MZjnk1a* mutants, which correlates with the reduced penetrance of bilateral *spaw* expression (Fig. 3B, 8C,I). Surprisingly and despite normal *spaw* expression in the left LPM (Fig. 4G) *MZjnk2* mutants also displayed a failure in anterior propagation of *lft1* along the midline, similar to *MZjnk1b* and *MZjnk1a*;*MZjnk1b* mutants (Fig. 8F,I). *lft1* propagation is also compromised in *MZjnk1a;MZjnk1b;Zjnk2* mutants, comparably to single *MZjnk1* or *MZjnk2* mutants (Fig. 8G,I). In *MZjnk3* mutants *lft1* expression is unaffected (Fig. 8H,I), correlating with normal *spaw* expression (Fig. 7G). However, this does not account for the bilateral expression of *pitx2c* in *MZjnk3* (Fig. 7H) and may suggest multiple roles for jnk genes, potentially outside of KV in the establishment of laterality.

In conclusion, all *jnk* family members play overlapping and specific roles in establishing the embryonic left-right axis. *jnk1a*, *jnk1b* and *jnk2* are required for normal nodal cilial length and it appears they may also be important in cilial motility as *jnk1a*, *jnk1b* and *jnk3* appear to have much greater reductions in KV flow relative to cilial shortening. For *jnk1b* this translates to abnormal bilateral expression of *spaw*, with an additional effect when *jnk2* is also inactivated. This appears to be related to abnormal midline barrier function as *lft1* is caudally restricted in these mutants. There is an increase in the proportion of embryos lacking *pitx2c* expression in *MZjnk1a;MZjnk1b;Zjnk2* mutants but it seems that the mechanisms that maintain left-sided *pitx2c* are intact in these mutants as the frequency of bilateral *pitx2c* expression that might be expected based on *spaw* expression is not seen in these mutants (compare Fig. 6B with Fig. 6A) and asymmetrical organ placement is maintained (Fig. 6C-D).

In contrast *jnk3* plays a minor role in KV development and function. Although loss of *jnk3* does not affect cilial length, there is a reduction in KV flow. However, despite this, normal *spaw* expression is established but surprisingly, there is a marked increase in bilateral *pitx2c* expression, even though midline barrier function appears normal. Whilst development of the heart is unaffected, abdominal organ development is strongly affected, with bilateral liver and pancreatic anlagen in *MZjnk3* mutants occurring at a frequency comparable to that of bilateral *pitx2c* expression.

DISCUSSION

We have characterised the roles of the *jnk* genes in establishing left-right asymmetry and shown, as previously suggested that *jnk1* promotes nodal cilial length (Gao et al., 2017), but that this role is shared by *jnk2* and together, both *jnk1* and *jnk2* are required for normal KV function (Fig. 5, Fig. S5). How *jnk* co-ordinates cilia length remains an open question as numerous proteins regulate cilia length at the level of post-translational modification. One interesting candidate, the JNK-interacting protein-1 (JIP1), is a regulator of JNK signalling and a cargo protein for the microtubular motor Kinesin-1 that is required for axon elongation (Dajas-Bailador et al., 2008). Alternatively, *jnk1/2* may regulate transcription factors involved in ciliogenesis such as *Rfx3* or *Foxj1* (Alten et al., 2012; Bonnafe et al., 2004) in response to developmental signals. In zebrafish, upstream of *foxj1a*, Notch signalling is critical in regulating nodal cilia length: over activity increases cilia length, whilst *deltaD* mutants have shorter cilia (40% reduction), a dramatic reduction in nodal flow and disruption to *spaw* and *pitx2* expression (Lopes et al., 2010). *foxj1* is also regulated by FGF signalling with *fgfr4* morphants displaying a 26% reduction in cilia length (Gao et al., 2017; Neugebauer et al., 2009). The micro-RNA *miR103/107* appears to regulate ciliogenesis downstream of *foxj1a*, acting on a cohort of genes including those involved in cilia assembly (Heigwer et al., 2020). *miR103/107* morphants also display shorter cilia (20% reduction) and disrupted asymmetric organ positioning (Heigwer et al., 2020). Importantly, where nodal cilia are either excessively long or significantly shorter, expression of *spaw* and *pitx2* are disrupted, suggesting a window of optimum nodal cilial length. (Lopes et al., 2010). Despite a comparably dramatic reduction in nodal cilia length in *MZjnk1a;MZjnk1b;Zjnk2* mutants (47%, Fig 5) and loss of KV function (Movie 6), organ looping is normal, suggesting that nodal cilia may function redundantly to establish organ laterality (Fig. S6). Of note, whilst *fgfr1* morphants have shortened nodal cilia, they also display a curved body axis, a more overt readout of cilial defects, which we did not observe in any *jnk* mutant (Fig. 4, Fig. 5, Fig. 7, Fig. S4)

(Neugebauer et al., 2009; Santos-Ledo et al., 2020). The absence of such obvious morphological defects in *jnk* mutants suggests different programmes may generate distinct classes of cilia and that the role of *jnk* may be specific to nodal or more generally, motile cilia.

Nodal cilia length, orientation and position in the node is critical for the generation of nodal flow, the proposed symmetry breaking event that establishes left-sided *Nodal* (Amack, 2014; Antic et al., 2010; Borovina et al., 2010; Minegishi et al., 2017; Nonaka et al., 1998; Nonaka et al., 2005; Song et al., 2010; Tabin, 2005). Whilst we have shown that *MZjnk1a;MZjnk1b;Zjnk2* mutants have no directional flow (Movie 6), our other mutants display reductions in nodal flow, yet directionality is maintained (Movies 1-5, 7-8), this contrasts with *MZvangl2* zebrafish and *Vangl2Vangl1* mutant mice in which normal cilia are incorrectly positioned resulting in irregular flow and laterality disturbances (Borovina et al., 2010; Song et al., 2010). *MZmyo1D* zebrafish mutants display similar disordered nodal flow patterns, together with more gross KV defects and ultimately disruptions to left-right asymmetry (Juan et al., 2018). Loss of a single copy of *vangl2* in *MZmyo1D* mutants partially rescues nodal flow, *spaw* expression and cardiac morphogenesis in a model whereby *myo1D* and *vangl2* interact to position nodal cilia (Juan et al., 2018). This KV-specific interaction may further support that different programmes exist to generate and position nodal cilia and that the *jnk* gene family is required for specification of cilia length.

Two possibilities have been suggested for the nodal flow-generated signal: morphogen flow, or the two-cilia model, where nodal flow activates mechanosensory cilia (Tabin and Vogan, 2003). In support of the two-cilia model, the calcium channel *pkd2* is proposed to facilitate left-sided calcium signalling that is at least partly required for heart jogging (Yuan et al., 2015). Importantly, *pkd2* functions both autonomously and non-autonomously in KV development (Jacinto et al., 2021). This highlights candidly that whilst the most overt phenotype of loss of *jnk1/2* activity may be shorter nodal cilia, *jnk* genes may act at multiple stages of KV function such as generation of cilia motility or sensation of nodal flow or may also function outside of KV in other tissues. Interestingly, our analysis in *MZjnk3* mutants (and also *MZjnk2* mutants), has shown that reduction of KV flow to less than 25% of wild-type levels is still sufficient to maintain left-sided *spaw* expression (Fig. 7). This indicates that either there is a threshold of KV flow required for KV function to establish the left signal and that this threshold is much lower than that generated in WT embryos, or that left-right axis establishment has a high degree of redundancy with other mechanisms, which may lie outside of KV (Fig. S6). There is some evidence for a minimal flow threshold within the

Node; as as few as two motile cilia have been shown to be sufficient to generate a left-sided Nodal signal in mice (Shinohara et al., 2012), whilst the minimal number of functional cilia in zebrafish required for correct organ placement has been suggested to be 29 out of approximately 200 (Sampaio et al., 2014). The shortening of the *lft1* expression in *jnk1* and *jnk2* mutants further supports that these genes may act not only in the KV, but also potentially downstream of *spaw* (Smith et al., 2011), possibly through a cilia-dependent mechanism at the midline (Shylo et al., 2018, preprint).

Our work supports an emerging viewpoint that certain organs possess intrinsic mechanisms that drive asymmetric morphogenesis. Loss of *spaw* does not lead to a loss of heart looping and a dextral bias is still maintained (Noël et al., 2013), similarly in mice, *Nodal* is dispensable for the morphogenesis of the heart tube itself (Desgrange et al., 2020; Le Garrec et al., 2017). This study, together with others, supports potential organ-specific mechanisms by demonstrating a disconnect between mesoderm and endodermal laterality (Fig. 7, Fig. S6).(Hochgreb-Hägele et al., 2013; Lopes et al., 2010; Noël et al., 2013; Sampaio et al., 2014) We have shown that *MZjnk3* embryos initially establish a left-right axis, a robust midline and that heart jogging is normal, yet a significant proportion of embryos develop bilateral guts (Fig. 7, Fig. 8) a similar organ laterality phenotype observed in *deltaD* and *lamb1a* mutants (Hochgreb-Hägele et al., 2013; Lopes et al., 2010).

Together with left-right asymmetry, deposition of ECM components such as laminins their and turnover by matrix metalloproteinases, regulated by the transcription factor *hand2,* are necessary for asymmetric gut looping (Hochgreb-Hägele et al., 2013; Yin et al., 2010). *hand2* mutants have bilateral guts arising from failure in the necessary asymmetric cell rearrangements of the LPM (Yin et al., 2010). It is therefore tempting to speculate that *jnk3* may have a role in regulating *hand2* expression which, coupled with our previous report for a role in which *jnk1a* regulates *hand2* expression in cardiac progenitors (Santos-Ledo et al., 2020), may suggest *jnk* family members have organ-specific or potentially germ-layer-specific roles in regulating *hand2* activity. Additionally, the single *JNK* gene in *Drosophila* is required for anterior midgut looping (Taniguchi et al., 2007) which may suggest a partially conserved role. A further explanation for the *MZjnk3* phenotype is suggested by the interesting observation that severity of reduction of nodal flow in the KV appears linked to the impact on endodermal laterality (Sampaio et al., 2014). This would suggest a KV-dependent, *spaw*-independent mechanism functions to promote gut looping morphogenesis.

Bilateral *pitx2c* expression in *MZjnk3* mutants, despite normal *spaw* and *lft1* expression is reminiscent of exposure of embryos to retinoic acid (Tsukui et al., 1999) possibly supporting cross-talk between left-right and antero-posterior axis establishment (Kawakami et al., 2005). Our data could also suggest that there may be an alternative, late acting midline barrier that is defective in *MZjnk3* mutants. Another possibility may be that in *MZjnk3* mutants, the right LPM is receptive to *nkx2.5* binding of the *pitx2* left side enhancer (ASE) (Shiratori et al., 2001) independent of right-sided *spaw* activity, allowing maintenance of bilateral *pitx2c*. However, the specific role that *pitx2* plays in zebrafish is unclear as loss of *pitx2* does not impact heart or gut looping (Ji et al., 2016). Furthermore, *Pitx2* mutant mice have been reported to have initially normal organ looping but develop more complex heart defects that may be independent of global left-right asymmetry (Ai et al., 2006; Gage et al., 1999; Lin et al., 1999; Lu et al., 1999). These observations may suggest that the endodermal phenotype in *MZjnk3* is independent of *pitx2*c. A further characterisation of brain asymmetry may also shed light on whether there is a potentially ectoderm-specific mechanism to promote asymmetry of the habenulae (Gamse et al., 2003) or whether this is tightly coupled to asymmetric *spaw* expression in the embryo.

From these observations it is clear that multiple pathways function during left-right axis establishment although their hierarchy remains unresolved; exemplified in zebrafish by a *pitx2*-independent, KV function-dependent cascade, for which *elovl6* is a known gene (Ji et al., 2016). Several other mechanisms, independent of nodal flow, have been proposed to establish left-right asymmetry, (Levin, 2003; Tabin, 2005) possibly even as early as the first cell division. Injection of dextran into one cell at the 2-cell stage in zebrafish results in a lineage labelling of one side of the embryo (Noël et al., 2013), whilst in *Xenopus*, abolishment of asymmetric localisation of 14-3-3E during the first cell division results in laterality disturbances (Bunney et al., 2003). Secondly, a mutation in *atp1a1a.1*, a component of the Na^+/K^+ transporter, presents with laterality defects, but KV structure and function appear normal (Ellertsdottir et al., 2006). Inhibition of the Na^+/K^+ pump with the chemical inhibitor Ouabain between 3-11hpf in zebrafish also results in laterality defects (Ellertsdottir et al., 2006) and may define a critical window as later treatment between 10-13hpf results in KV morphogenesis defects (Juan et al., 2018), possibly suggesting that early activity of this ion pump is important for left-right asymmetry at least functioning in parallel with Nodal signalling (Fig. S6, green). Finally, *jnk* genes may also function outside of the KV to repress a right-sided factor, such as the transcription factor *Snail* (Isaac et al., 1997). However, the existence and role of such a factor remains controversial (Castroviejo et al., 2020; Ocaña et al., 2017; Tessadori et al., 2020). Organ asymmetry remains highly

stereotypical in *MZjnk1a*;*MZjnk1b*;*Zjnk2* mutants, despite a loss of nodal flow (Movie 6) and disruption to *spaw* expression (Fig. 6A), suggesting that nodal flow is not required as the critical symmetry breaking event as other mechanisms recover initially defective cues in the early embryo (Fig. S6). Further characterisation of left-right patterning in the heart prior to jogging using markers such as *lft2* and *bmp4* (Chocron et al., 2007; Smith et al., 2008; Veerkamp et al., 2013) may uncover whether disruption to asymmetric *spaw* is recovered.

Examination of a repertoire of vertebrate model organisms highlights that nodal-cilia-independent mechanisms may be commonplace but not yet fully elucidated (Hamada and Tam, 2020). Whilst zebrafish, Xenopus and mouse possess a ciliated LRO (left-right organiser), there are no luminally positioned motile cilia in the chick LRO (Hensen's node) and loss of C2Cd3 a gene essential for ciliogenesis does not result in disruption to laterality (Chang et al., 2014), instead asymmetric cell movements have been proposed to break bilateral symmetry (Cui et al., 2009; Gros et al., 2009). Furthermore, the observations regarding nodal cilia have been extend to pig embryos, with the suggestion that the node is not large enough to generate fluid flow or even exist (Gros et al., 2009). Comparisons with non-vertebrate model organisms may provide insightful, exemplified by role of *myo1D* in establishment of laterality in both *Drosophila* and zebrafish (Juan et al., 2018).

Both genetic and cell-based studies have suggested that *JNK* family members are key components of the PCP pathway (Boutros et al., 1998; Kim and Han, 2005). However, many of these have examined only a single member of the *JNK* family, used pharmacological methods or injected antisense-morpholino oligonucleotides, rather characterise stable mutant lines. Although unable to examine total *jnk* nulls due to our *jnk2* and *jnk3* alleles being generated in *trans*, this and our previous study (Santos-Ledo et al., 2020) have failed to reveal even a mild convergent-extension phenotype in *jnk* mutants, the hallmark of PCP signalling disturbances (Jessen et al., 2002; Park and Moon, 2002; Solnica-Krezel et al., 1996). Furthermore, we observed no PCP-related node abnormalities, such as mal-positioning or -distribution of cilia (Borovina et al., 2010; Wang et al., 2011). Thus, it is possible that *JNK* activity is not a definitive requirement for PCP signalling. Supporting this, combinatorial *Jnk* mouse mutants, or treatment of embryos heterozygous for PCP mutations with a JNK inhibitor, do not display defects in convergent-extension (Kuan et al., 1999; Ybot-Gonzalez et al., 2007). Furthermore, whilst suppression of JNK activity in *Drosophila* is able to rescue defective PCP signalling, loss of JNK activity alone only produces a subtle PCP phenotype in the eye (Boutros et al., 1998; Paricio et al., 1999) and in *Xenopus* explants, *JNK1* is not sufficient to regulate Wnt5a-driven convergent-extension (Yamanaka et al.,

2002). However, in many of these experimental contexts, removal of kinase activity upstream of JNK signalling, such as *misshapen/TNIK* (Köppen et al., 2006; Paricio et al., 1999) or *MKK7* (Yamanaka et al., 2002), does result in classical PCP phenotypes. In summary, this suggests that although JNK activity is a readout of active PCP signalling (Boutros et al., 1998; Li et al., 1999; Moriguchi et al., 1999), the activity of JNK itself may not be critical to the generation of planar cell polarity and that upstream factors may be more important (Paricio et al., 1999; Yamanaka et al., 2002) or show redundancy with *JNK* genes.

Establishment of laterality is proposed to be a sequential process, through an initial symmetry breaking event commonly thought to be at the node, which is amplified to a *Nodal* homolog during early development and relayed subsequently through genes such as *Pitx2* to the organ anlagen to drive asymmetric morphogenesis. In this study we have characterised the role of the *jnk* family members in the formation, function and downstream effects of nodal cilia in zebrafish. We have shown that *jnk1/jnk2* function to specify nodal cilia length, promote nodal flow and establish the *lft1* midline barrier, but that this is dispensable for the correct establishment of organ asymmetry and suggests other node-independent mechanisms are able to recover this early phenotype (Fig. S6). We have also identified a novel, later requirement for *jnk3* to maintain lateralised *pitx2c* expression which may either directly or indirectly promote asymmetric morphogenesis of the endoderm. Together, this demonstrates that multiple mechanisms, both, *jnk*-dependent and -independent act redundantly at different stages during vertebrate axis establishment ensuring robust, asymmetric organ morphogenesis.

Materials and Methods

Zebrafish handling and maintenance

The following previously described zebrafish lines were used in this study: WT (AB), *jnk1a*^{n2} (*mapk8a*) and *jnk1b*^{n3} (*mapk8b*) (Santos-Ledo et al., 2020). All procedures and experimental protocols were in accordance with UK Home Office and Newcastle University (Project License P25F4F0F4). Embryos were obtained from natural pairwise mating and reared in standard conditions. Embryos were raised in Embryo Medium (E3) at 28.5°C and staged according to (Kimmel et al., 1995).

Generation of *jnk2* and *jnk3* mutants

jnk2 (mapk9, ENSDARG00000077364, ZDB-GENE-091117-28) *and jnk3 (mapk10,* ENSDARG00000102730*,* ZDB-GENE-051120-117) zebrafish mutants were generated using CRISPR-Cas9-mediated mutagenesis (Hwang et al., 2013). gRNAs were identified using CrisprScan (Moreno-Mateos et al., 2015). gRNAs and Cas9 RNA were synthesized according to previously published protocols (Gagnon et al., 2014) and injected at the 1-cell stage into embryos obtained from an in-cross of WT (AB) adults (F0 generation). The 20bp deletion in Exon 3 of *jnk2* (allele designation *mapk9*^{n4}) was generated using the single gRNA: 5'-ATTTAGGTGACACTATAGCAATCTTCACATCCAGGACGTTTTAGAGCTAGAAATAGCAAG -3' and genotyped using Forward: 5'- TTAAAGGGGATTGAGGAACAAA-3' and Reverse: 5'-GTTAAGGGGACGTACGTTCTTG-3' primers in a standard GoTaq G2 (Promega M784B) PCR with an annealing temperature of 58^{o}C and 34 cycles. The mutation destroys a DdeI restriction enzyme site (New England Biolabs R1075). The 4bp deletion in Exon 5 of *jnk3* (allele designation *mapk10*^{n5}) was generated using the single gRNA: 5'-ATTTAGGTGACACTATAGGCCACATTTCTGTCCAGGAGTTTTAGAGCTAGAAATAGCAA G-3' and genotyped using Forward: 5'- AATTCCCATCTTGTGTTTCAGG-3' and Reverse: 5'-TTTTGGGGAAAACCTGACTCTAA -3' primers in a standard GoTaq G2 PCR with an annealing temperature of 58^{o}C and 34 cycles. The mutation destroys a BstNI restriction enzyme site (New England Biolabs R1068). F0 adults identified as carrying desired mutations were out-crossed to WT animals prior to generation of homozygous mutant lines. Where lines were derived from multiple rounds of in-crossing, a minimum of 6 different breeding pairs were used to establish the next generation. Reduction in mRNA levels in *MZjnk2* or *MZjnk3* mutants was confirmed by RT-PCR using primers and protocols previously described (Santos-Ledo et al., 2020).

Immunohistochemistry

Fixed embryos were serially rehydrated from 100% MeOH into PBST (0.2% Tween-20 (Sigma P2287) in 1x PBS (Oxoid BR0014G)), washed 3 times in 0.2% Triton-X (Sigma T8787) in 1x PBS (PBSTx) and then incubated in blocking buffer for 1hr at room temperature in 5% Sheep Serum (Gibco, 16070-096), 10mg/mL Bovine Serum Albumin (A2153, Sigma), 1% DMSO (D4540, Sigma) in PBSTx before an overnight incubation at 4^{O}C with gentle agitation with the following primary antibodies: Mouse anti-Acetylated Tubulin (T6793, Sigma, 1:500) and Rabbit anti-PKC ζ (aPKC) (sc-216, Santa Cruz, 1:400) in blocking buffer

(Amack et al., 2007). The next day, embryos were rinsed extensively in PBSTx, before a further overnight incubation at 4^{o}C with gentle agitation with the following secondaries: Alexa488-conjugated Donkey anti-Mouse (Invitrogen A21202, 1:200) and Alexa647-conjugated Donkey anti-Rabbit (Invitrogen A31573, 1:200) in blocking buffer. Embryos were washed extensively on day three before dissection or embedding. Representative images of Kupffer's Vesicle were taken using a Nikon A1 inverted confocal using a 40x objective.

Quantification of cilial length

Embryos were embedded in 1.5% low melting agarose (ThermoFisher Scientific R0801) in PBS and imaged in an Axiotome microscope using a 40x objective. An image stack was recorded and used for quantification. Stacks were opened in Fiji where the number of cilia and their position relative to the anterior and posterior parts of the Kupffer's vesicle were quantified (Wang et al., 2011). Then, the XY coordinates of all cilia were recorded in every slice. The total length of the cilia was obtained as previously described (Dummer et al., 2016). The XY coordinates were translated to µm assuming the following equivalencies: 1 pixel = 0.1623 µm, 1 slice = 0.4 µm.

Quantification of fluid flow in Kupffer's Vesicle by microbead injection

Analysis of nodal flow was carried out as previously described (Wang et al., 2013), using TransFluoSpheres beads of 1µm diameter (Invitrogen T8880). High speed movies were acquired using an Axiotome microscope with either a 40x or 60x objective attached to an IMPERX high speed camera with Video Savant 4.0 software (Multipix Ltd, UK). The frame rate of acquired movies was 207 frames per second. Stacks were imported into Fiji (Schindelin et al., 2012), the notochord oriented to the top of the image and the quadrants denoted. Every fifth frame representing approximately 0.0125s were used to track bead speed by the Manual Tracking plugin. Beads were tracked that remained in the focal plane of the movie for ≥50 frames Average speeds of beads were then calculated for the duration of tracking. (Wang et al., 2011; Wang et al., 2013).

mRNA *in situ* hybridisation

Embryos older than 24hpf for use in *in situ* hybridisation, were transferred into E3 medium containing 0.003% 1-phenyl 2-thiourea (PTU, Sigma P7629) to inhibit pigment formation and aid imaging. Embryos were fixed overnight in 4% paraformaldehyde (PFA, P6148, Sigma) in 1x Phosphate Buffered Saline, washed 3 times in PBST for 5 minutes at room temperature and then serially washed into 100% MeOH for long term storage at -20^{O}C. Wholemount *in situ* hybridisation was carried out according to standard protocols (Thisse and Thisse, 2008). The following, previously published probes were used: *dand5* (Hashimoto et al., 2004), *spaw* (Long et al., 2003), *myl7* (Yelon et al., 1999), *foxa3* (Odenthal and Nüsslein-Volhard, 1998), *lft1* (Bisgrove et al., 1999), *pitx2c* (Yan et al., 1999).

Quantification of *lft1* domain

ISHs were imaged laterally using a Zeiss AxioPlan. Images were pooled and blinded using Image J Blind_Analysis plugin as previously described (Derrick et al., 2021) and imported into Fiji (Schindelin et al., 2012). Using the Freehand Line tool, the length of the domain with continuous expression was measured from the caudal tip to the anterior extreme was measured. Embryos without any visible *lft1* expression were discounted from analysis.

Statistical Analysis

No statistical tests were used to formally predetermine sample size, but the number of biological replicates were based on published studies and defined *a priori*. For all experiments where n was based on the individual embryo (e.g. KV flow), they were derived from at least 3 different clutches from distinct breeding pairs. For population analysis of laterality markers or organ asymmetry, N was represented by the clutch, and each clutch derived from 3 distinct breeding pairs. Statistical tests were carried out in Prism (Graphpad Prism, USA).

ACKNOWLEDGEMENTS

The authors gratefully acknowledge the BioImaging Unit and Aquarium Technical team for their support & assistance in this work.

COMPETING INTERESTS

The authors declare no competing interests.

FUNDING

This project was funded by the British Heart Foundation, grant number PG/15/58/31611 awarded to BC and DJH. The funders had no role in study design, data collection and analysis, decision to publish, or preparation of the manuscript.

REFERENCES

Ai, D., Liu, W., Ma, L., Dong, F., Lu, M.-F., Wang, D., Verzi, M. P., Cai, C., Gage, P. J., Evans, S., et al. (2006). Pitx2 regulates cardiac left-right asymmetry by patterning second cardiac lineage-derived myocardium. Dev. Biol. 296, 437–449.

Alten, L., Schuster-Gossler, K., Beckers, A., Groos, S., Ulmer, B., Hegermann, J., Ochs, M. and Gossler, A. (2012). Differential regulation of node formation, nodal ciliogenesis and cilia positioning by Noto and Foxj1. Development 139, 1276–1284.

Amack, J. D. (2014). Salient features of the ciliated organ of asymmetry. Bioarchitecture 4, 6–15.

Amack, J. D., Wang, X. and Yost, H. J. (2007). Two T-box genes play independent and cooperative roles to regulate morphogenesis of ciliated Kupffer's vesicle in zebrafish. Dev. Biol. 310, 196–210.

Antic, D., Stubbs, J. L., Suyama, K., Kintner, C., Scott, M. P. and Axelrod, J. D. (2010). Planar cell polarity enables posterior localization of nodal cilia and left-right axis determination during mouse and Xenopus embryogenesis. PLoS One 5, e8999.

Bisgrove, B. W., Essner, J. J. and Yost, H. J. (1999). Regulation of midline development by antagonism of lefty and nodal signaling. Development 126, 3253–3262.

Blum, M. and Ott, T. (2018). Animal left-right asymmetry. Curr. Biol. 28, R301–R304.

Bonnafe, E., Touka, M., AitLounis, A., Baas, D., Barras, E., Ucla, C., Moreau, A., Flamant, F., Dubruille, R., Couble, P., et al. (2004). The transcription factor RFX3 directs nodal cilium development and left-right asymmetry specification. Mol. Cell. Biol. 24, 4417–4427.

Borovina, A., Superina, S., Voskas, D. and Ciruna, B. (2010). Vangl2 directs the posterior tilting and asymmetric localization of motile primary cilia. Nat. Cell Biol. 12, 407–412.

Boutros, M., Paricio, N., Strutt, D. I. and Mlodzik, M. (1998). Dishevelled activates JNK and discriminates between JNK pathways in planar polarity and wingless signaling. Cell 94, 109–118.

Bunney, T. D., De Boer, A. H. and Levin, M. (2003). Fusicoccin signaling reveals 14-3-3 protein function as a novel step in left-right patterning during amphibian embryogenesis. Development 130, 4847–4858.

Campione, M., Steinbeisser, H., Schweickert, A., Deissler, K., van Bebber, F., Lowe, L. A., Nowotschin, S., Viebahn, C., Haffter, P., Kuehn, M. R., et al. (1999). The homeobox gene Pitx2: mediator of asymmetric left-right signaling in vertebrate heart and gut looping. Development.

Castroviejo, N., Ocaña, O. H., Rago, L., Coskun, H., Arcas, A., Galcerán, J. and Nieto, M. A. (2020). Reply to: Zebrafish prrx1a mutants have normal hearts. Nature 585, E17–E19.

Chang, C.-F., Schock, E.N., O'Hare, E.A., Dodgson, J., Cheng, H.H., Muir, W.M., Edelmann, R.E., Delany, M.E., Brugmann, S.A., 2014. The cellular and molecular etiology of the craniofacial defects in the avian ciliopathic mutant talpid2. Development 141, 3003–3012. doi:10.1242/dev.105924

Chen, J. N., van Eeden, F. J., Warren, K. S., Chin, A., Nüsslein-Volhard, C., Haffter, P. and Fishman, M. C. (1997). Left-right pattern of cardiac BMP4 may drive asymmetry of the heart in zebrafish. Development 124, 4373–4382.

Chocron, S., Verhoeven, M. C., Rentzsch, F., Hammerschmidt, M. and Bakkers, J. (2007). Zebrafish Bmp4 regulates left-right asymmetry at two distinct developmental time points. Dev. Biol. 305, 577–588.

Cui, C., Little, C.D., Rongish, B.J., 2009. Rotation of organizer tissue contributes to left-right asymmetry. Anat Rec (Hoboken) 292, 557–561. doi:10.1002/ar.20872

Dajas-Bailador, F., Jones, E. V. and Whitmarsh, A. J. (2008). The JIP1 scaffold protein regulates axonal development in cortical neurons. Curr. Biol. 18, 221–226.

Davis, R. J. (2000). Signal transduction by the JNK group of MAP kinases. Cell 103, 239–252.

Derrick, C. J., Sánchez-Posada, J., Hussein, F., Tessadori, F., Pollitt, E. J. G., Savage, A. M., Wilkinson, R. N., Chico, T. J., van Eeden, F. J., Bakkers, J., et al. (2021). Asymmetric Hapln1a drives regionalised cardiac ECM expansion and promotes heart morphogenesis in zebrafish development. Cardiovasc. Res.

Desgrange, A., Le Garrec, J.-F., Bernheim, S., Bønnelykke, T. H. and Meilhac, S. M. (2020). Transient nodal signaling in left precursors coordinates opposed asymmetries shaping the heart loop. Dev. Cell 55, 413–431.e6.

Dummer, A., Poelma, C., DeRuiter, M. C., Goumans, M.-J. T. H. and Hierck, B. P. (2016). Measuring the primary cilium length: improved method for unbiased high-throughput analysis. Cilia 5, 7.

Ellertsdottir, E., Ganz, J., Dürr, K., Loges, N., Biemar, F., Seifert, F., Ettl, A.-K., Kramer-Zucker, A. K., Nitschke, R. and Driever, W. (2006). A mutation in the zebrafish Na,K-ATPase subunit atp1a1a.1 provides genetic evidence that the sodium potassium pump contributes to left-right asymmetry downstream or in parallel to nodal flow. Dev. Dyn. 235, 1794–1808.

Essner, J. J., Branford, W. W., Zhang, J. and Yost, H. J. (2000). Mesendoderm and left-right brain, heart and gut development are differentially regulated by pitx2 isoforms. Development 127, 1081–1093.

Essner, J. J., Amack, J. D., Nyholm, M. K., Harris, E. B. and Yost, H. J. (2005). Kupffer's vesicle is a ciliated organ of asymmetry in the zebrafish embryo that initiates left-right development of the brain, heart and gut. Development 132, 1247–1260.

Gage, P. J., Suh, H. and Camper, S. A. (1999). Dosage requirement of Pitx2 for development of multiple organs. Development 126, 4643–4651.

Gagnon, J. A., Valen, E., Thyme, S. B., Huang, P., Akhmetova, L., Pauli, A., Montague, T. G., Zimmerman, S., Richter, C. and Schier, A. F. (2014). Efficient mutagenesis by Cas9 protein-mediated oligonucleotide insertion and large-scale assessment of single-guide RNAs. PLoS One 9, e98186.

Gamse, J. T., Thisse, C., Thisse, B. and Halpern, M. E. (2003). The parapineal mediates left-right asymmetry in the zebrafish diencephalon. Development 130, 1059–1068.

Gao, Q., Zhang, J., Wang, X., Liu, Y., He, R., Liu, X., Wang, F., Feng, J., Yang, D., Wang, Z., et al. (2017). The signalling receptor MCAM coordinates apical-basal polarity and planar cell polarity during morphogenesis. Nat. Commun. 8, 15279.

Grimes, D. T. and Burdine, R. D. (2017). Left-Right Patterning: Breaking Symmetry to Asymmetric Morphogenesis. Trends Genet. 33, 616–628.

Gros, J., Feistel, K., Viebahn, C., Blum, M., Tabin, C.J., 2009. Cell movements at Hensen's node establish left/right asymmetric gene expression in the chick. Science 324, 941–944. doi:10.1126/science.1172478

Gupta, S., Barrett, T., Whitmarsh, A. J., Cavanagh, J., Sluss, H. K., Dérijard, B. and Davis, R. J. (1996). Selective interaction of JNK protein kinase isoforms with transcription factors. EMBO J. 15, 2760–2770.

Hamada, H., Tam, P., 2020. Diversity of left-right symmetry breaking strategy in animals. [version 1; peer review: 2 approved]. F1000Res. 9. doi:10.12688/f1000research.21670.1

Hashimoto, H., Rebagliati, M., Ahmad, N., Muraoka, O., Kurokawa, T., Hibi, M. and Suzuki, T. (2004). The Cerberus/Dan-family protein Charon is a negative regulator of Nodal signaling during left-right patterning in zebrafish. Development 131, 1741–1753.

Hashimoto, M., Shinohara, K., Wang, J., Ikeuchi, S., Yoshiba, S., Meno, C., Nonaka, S., Takada, S., Hatta, K., Wynshaw-Boris, A., et al. (2010). Planar polarization of node cells determines the rotational axis of node cilia. Nat. Cell Biol. 12, 170–176.

Heigwer, J., Kutzner, J., Haeussler, M., Burkhalter, M. D., Draebing, T., Juergensen, L., Katus, H. A., Philipp, M., Westhoff, J. H. and Hassel, D. (2020). miR-103/107 regulates left-right asymmetry in zebrafish by modulating Kupffer's vesicle development and ciliogenesis. Biochem. Biophys. Res. Commun. 527, 432–439.

Hochgreb-Hägele, T., Yin, C., Koo, D. E. S., Bronner, M. E. and Stainier, D. Y. R. (2013). Laminin β1a controls distinct steps during the establishment of digestive organ laterality. Development 140, 2734–2745.

Homsy, J. G., Jasper, H., Peralta, X. G., Wu, H., Kiehart, D. P. and Bohmann, D. (2006). JNK signaling coordinates integrin and actin functions during Drosophila embryogenesis. Dev. Dyn. 235, 427–434.

Horne-Badovinac, S., Rebagliati, M. and Stainier, D. Y. R. (2003). A cellular framework for gut-looping morphogenesis in zebrafish. Science 302, 662–665.

Hwang, W. Y., Fu, Y., Reyon, D., Maeder, M. L., Tsai, S. Q., Sander, J. D., Peterson, R. T., Yeh, J.-R. J. and Joung, J. K. (2013). Efficient genome editing in zebrafish using a CRISPR-Cas system. Nat. Biotechnol. 31, 227–229.

Isaac, A., Sargent, M. G. and Cooke, J. (1997). Control of vertebrate left-right asymmetry by a snail-related zinc finger gene. Science 275, 1301–1304.

Jacinto, R., Sampaio, P., Roxo-Rosa, M., Pestana, S. and Lopes, S. S. (2021). Pkd2 affects cilia length and impacts LR flow dynamics and dand5. Front. Cell Dev. Biol. 9, 624531.

Jessen, J. R., Topczewski, J., Bingham, S., Sepich, D. S., Marlow, F., Chandrasekhar, A. and Solnica-Krezel, L. (2002). Zebrafish trilobite identifies new roles for Strabismus in gastrulation and neuronal movements. Nat. Cell Biol. 4, 610–615.

Ji, Y., Buel, S. M. and Amack, J. D. (2016). Mutations in zebrafish pitx2 model congenital malformations in Axenfeld-Rieger syndrome but do not disrupt left-right placement of visceral organs. Dev. Biol. 416, 69–81.

Juan, T., Géminard, C., Coutelis, J.-B., Cerezo, D., Polès, S., Noselli, S. and Fürthauer, M. (2018). Myosin1D is an evolutionarily conserved regulator of animal left-right asymmetry. Nat. Commun. 9, 1942.

Kawakami, Y., Raya, A., Raya, R. M., Rodríguez-Esteban, C. and Izpisúa Belmonte, J. C. (2005). Retinoic acid signalling links left-right asymmetric patterning and bilaterally symmetric somitogenesis in the zebrafish embryo. Nature 435, 165–171.

Kennedy, M. P., Omran, H., Leigh, M. W., Dell, S., Morgan, L., Molina, P. L., Robinson, B. V., Minnix, S. L., Olbrich, H., Severin, T., et al. (2007). Congenital heart disease and other heterotaxic defects in a large cohort of patients with primary ciliary dyskinesia. Circulation 115, 2814–2821.

Kim, G.-H. and Han, J.-K. (2005). JNK and ROKalpha function in the noncanonical Wnt/RhoA signaling pathway to regulate Xenopus convergent extension movements. Dev. Dyn. 232, 958–968.

Kimmel, C. B., Ballard, W. W., Kimmel, S. R., Ullmann, B. and Schilling, T. F. (1995). Stages of embryonic development of the zebrafish. Dev. Dyn. 203, 253–310.

Köppen, M., Fernández, B. G., Carvalho, L., Jacinto, A. and Heisenberg, C.-P. (2006). Coordinated cell-shape changes control epithelial movement in zebrafish and Drosophila. Development 133, 2671–2681.
Kuan, C. Y., Yang, D. D., Samanta Roy, D. R., Davis, R. J., Rakic, P. and Flavell, R. A. (1999). The Jnk1 and Jnk2 protein kinases are required for regional specific apoptosis during early brain development. Neuron 22, 667–676.
Kupffer, C (1868). Beobachtungea uber die Entwicklung der Knochenfische. Arch. Mikrob. Anat.
Le Garrec, J.-F., Domínguez, J. N., Desgrange, A., Ivanovitch, K. D., Raphaël, E., Bangham, J. A., Torres, M., Coen, E., Mohun, T. J. and Meilhac, S. M. (2017). A predictive model of asymmetric morphogenesis from 3D reconstructions of mouse heart looping dynamics. Elife 6,.
Lenhart, K. F., Holtzman, N. G., Williams, J. R. and Burdine, R. D. (2013). Integration of nodal and BMP signals in the heart requires FoxH1 to create left-right differences in cell migration rates that direct cardiac asymmetry. PLoS Genet. 9, e1003109.
Levin, M. (2003). Motor protein control of ion flux is an early step in embryonic left-right asymmetry. Bioessays 25, 1002–1010.
Li, L., Yuan, H., Xie, W., Mao, J., Caruso, A. M., McMahon, A., Sussman, D. J. and Wu, D. (1999). Dishevelled proteins lead to two signaling pathways. Regulation of LEF-1 and c-Jun N-terminal kinase in mammalian cells. J. Biol. Chem. 274, 129–134.
Lin, C. R., Kioussi, C., O'Connell, S., Briata, P., Szeto, D., Liu, F., Izpisúa-Belmonte, J. C. and Rosenfeld, M. G. (1999). Pitx2 regulates lung asymmetry, cardiac positioning and pituitary and tooth morphogenesis. Nature 401, 279–282.
Long, S., Ahmad, N. and Rebagliati, M. (2003). The zebrafish nodal-related gene southpaw is required for visceral and diencephalic left-right asymmetry. Development 130, 2303–2316.
Lopes, S. S., Lourenço, R., Pacheco, L., Moreno, N., Kreiling, J. and Saúde, L. (2010). Notch signalling regulates left-right asymmetry through ciliary length control. Development 137, 3625–3632.
Lu, M. F., Pressman, C., Dyer, R., Johnson, R. L. and Martin, J. F. (1999). Function of Rieger syndrome gene in left-right asymmetry and craniofacial development. Nature 401, 276–278.
Meno, C., Shimono, A., Saijoh, Y., Yashiro, K., Mochida, K., Ohishi, S., Noji, S., Kondoh, H. and Hamada, H. (1998). lefty-1 is required for left-right determination as a regulator of lefty-2 and nodal. Cell 94, 287–297.
Minegishi, K., Hashimoto, M., Ajima, R., Takaoka, K., Shinohara, K., Ikawa, Y., Nishimura, H., McMahon, A. P., Willert, K., Okada, Y., et al. (2017). A Wnt5 Activity Asymmetry and Intercellular Signaling via PCP Proteins Polarize Node Cells for Left-Right Symmetry Breaking. Dev. Cell 40, 439–452.e4.
Moreno-Mateos, M. A., Vejnar, C. E., Beaudoin, J.-D., Fernandez, J. P., Mis, E. K., Khokha, M. K. and Giraldez, A. J. (2015). CRISPRscan: designing highly efficient sgRNAs for CRISPR-Cas9 targeting in vivo. Nat. Methods 12, 982–988.
Moriguchi, T., Kawachi, K., Kamakura, S., Masuyama, N., Yamanaka, H., Matsumoto, K., Kikuchi, A. and Nishida, E. (1999). Distinct domains of mouse dishevelled are responsible for the c-Jun N-terminal kinase/stress-activated protein kinase activation and the axis formation in vertebrates. J. Biol. Chem. 274, 30957–30962.
Nakamura, T., Mine, N., Nakaguchi, E., Mochizuki, A., Yamamoto, M., Yashiro, K., Meno, C. and Hamada, H. (2006). Generation of robust left-right asymmetry in the mouse embryo requires a self-enhancement and lateral-inhibition system. Dev. Cell 11, 495–504.
Neugebauer, J. M., Amack, J. D., Peterson, A. G., Bisgrove, B. W. and Yost, H. J. (2009). FGF signalling during embryo development regulates cilia length in diverse epithelia. Nature 458, 651–654.
Noël, E. S., Verhoeven, M., Lagendijk, A. K., Tessadori, F., Smith, K., Choorapoikayil, S., den Hertog, J. and Bakkers, J. (2013). A Nodal-independent and tissue-intrinsic mechanism controls heart-looping chirality. Nat. Commun. 4, 2754.

Nonaka, S., Tanaka, Y., Okada, Y., Takeda, S., Harada, A., Kanai, Y., Kido, M. and Hirokawa, N. (1998). Randomization of left-right asymmetry due to loss of nodal cilia generating leftward flow of extraembryonic fluid in mice lacking KIF3B motor protein. Cell 95, 829–837.
Nonaka, S., Yoshiba, S., Watanabe, D., Ikeuchi, S., Goto, T., Marshall, W. F. and Hamada, H. (2005). De novo formation of left-right asymmetry by posterior tilt of nodal cilia. PLoS Biol. 3, e268.
Ocaña, O. H., Coskun, H., Minguillón, C., Murawala, P., Tanaka, E. M., Galcerán, J., Muñoz-Chápuli, R. and Nieto, M. A. (2017). A right-handed signalling pathway drives heart looping in vertebrates. Nature 549, 86–90.
Odenthal, J. and Nüsslein-Volhard, C. (1998). fork head domain genes in zebrafish. Dev. Genes Evol. 208, 245–258.
Paricio, N., Feiguin, F., Boutros, M., Eaton, S. and Mlodzik, M. (1999). The Drosophila STE20-like kinase misshapen is required downstream of the Frizzled receptor in planar polarity signaling. EMBO J. 18, 4669–4678.
Park, M. and Moon, R. T. (2002). The planar cell-polarity gene stbm regulates cell behaviour and cell fate in vertebrate embryos. Nat. Cell Biol. 4, 20–25.
Riesgo-Escovar, J. R., Jenni, M., Fritz, A. and Hafen, E. (1996). The Drosophila Jun-N-terminal kinase is required for cell morphogenesis but not for DJun-dependent cell fate specification in the eye. Genes Dev. 10, 2759–2768.
Roszko, I., Sawada, A. and Solnica-Krezel, L. (2009). Regulation of convergence and extension movements during vertebrate gastrulation by the Wnt/PCP pathway. Semin. Cell Dev. Biol. 20, 986–997.
Rudrapatna, V. A., Bangi, E. and Cagan, R. L. (2014). A Jnk-Rho-Actin remodeling positive feedback network directs Src-driven invasion. Oncogene 33, 2801–2806.
Sampaio, P., Ferreira, R. R., Guerrero, A., Pintado, P., Tavares, B., Amaro, J., Smith, A. A., Montenegro-Johnson, T., Smith, D. J. and Lopes, S. S. (2014). Left-right organizer flow dynamics: how much cilia activity reliably yields laterality? Dev. Cell 29, 716–728.
Santos-Ledo, A., Washer, S., Dhanaseelan, T., Eley, L., Alqatani, A., Chrystal, P. W., Papoutsi, T., Henderson, D. J. and Chaudhry, B. (2020). Alternative splicing of jnk1a in zebrafish determines first heart field ventricular cardiomyocyte numbers through modulation of hand2 expression. PLoS Genet. 16, e1008782.
Schindelin, J., Arganda-Carreras, I., Frise, E., Kaynig, V., Longair, M., Pietzsch, T., Preibisch, S., Rueden, C., Saalfeld, S., Schmid, B., et al. (2012). Fiji: an open-source platform for biological-image analysis. Nat. Methods 9, 676–682.
Schottenfeld, J., Sullivan-Brown, J. and Burdine, R. D. (2007). Zebrafish curly up encodes a Pkd2 ortholog that restricts left-side-specific expression of southpaw. Development 134, 1605–1615.
Shinohara, K., Kawasumi, A., Takamatsu, A., Yoshiba, S., Botilde, Y., Motoyama, N., Reith, W., Durand, B., Shiratori, H., Hamada, H., 2012. Two rotating cilia in the node cavity are sufficient to break left-right symmetry in the mouse embryo. Nat. Commun. 3, 622. doi:10.1038/ncomms1624
Shiraishi, I. and Ichikawa, H. (2012). Human heterotaxy syndrome – from molecular genetics to clinical features, management, and prognosis – . Circ. J. 76, 2066–2075.
Shiratori, H., Sakuma, R., Watanabe, M., Hashiguchi, H., Mochida, K., Sakai, Y., Nishino, J., Saijoh, Y., Whitman, M. and Hamada, H. (2001). Two-Step Regulation of Left–Right Asymmetric Expression of Pitx2. Mol. Cell 7, 137–149.
Shylo, N. A., Ramrattan, D. A. and Weatherbee, S. D. (2018). Presence of midline cilia supersedes the expression of Lefty1 in forming the midline barrier during the establishment of left-right asymmetry. BioRxiv.
Smith, K. A. and Uribe, V. (2021). Getting to the Heart of Left-Right Asymmetry: Contributions from the Zebrafish Model. J. Cardiovasc. Dev. Dis. 8,.
Smith, K. A., Chocron, S., von der Hardt, S., de Pater, E., Soufan, A., Bussmann, J., Schulte-Merker, S., Hammerschmidt, M. and Bakkers, J. (2008). Rotation and asymmetric development of the zebrafish heart requires directed migration of cardiac progenitor cells. Dev. Cell 14, 287–297.

Smith, K. A., Noël, E., Thurlings, I., Rehmann, H., Chocron, S. and Bakkers, J. (2011). Bmp and nodal independently regulate lefty1 expression to maintain unilateral nodal activity during left-right axis specification in zebrafish. PLoS Genet. 7, e1002289.
Solnica-Krezel, L., Stemple, D. L., Mountcastle-Shah, E., Rangini, Z., Neuhauss, S. C., Malicki, J., Schier, A. F., Stainier, D. Y., Zwartkruis, F., Abdelilah, S., et al. (1996). Mutations affecting cell fates and cellular rearrangements during gastrulation in zebrafish. Development 123, 67–80.
Song, H., Hu, J., Chen, W., Elliott, G., Andre, P., Gao, B. and Yang, Y. (2010). Planar cell polarity breaks bilateral symmetry by controlling ciliary positioning. Nature 466, 378–382.
Tabin, C. (2005). Do we know anything about how left-right asymmetry is first established in the vertebrate embryo? J Mol Histol 36, 317–323.
Tabin, C. J. and Vogan, K. J. (2003). A two-cilia model for vertebrate left-right axis specification. Genes Dev. 17, 1–6.
Taniguchi, K., Hozumi, S., Maeda, R., Ooike, M., Sasamura, T., Aigaki, T. and Matsuno, K. (2007). D-JNK signaling in visceral muscle cells controls the laterality of the Drosophila gut. Dev. Biol. 311, 251–263.
Tessadori, F., de Bakker, D. E. M., Barske, L., Nelson, N., Algra, H. A., Willekers, S., Nichols, J. T., Crump, J. G. and Bakkers, J. (2020). Zebrafish prrx1a mutants have normal hearts. Nature 585, E14–E16.
Thisse, C. and Thisse, B. (2008). High-resolution in situ hybridization to whole-mount zebrafish embryos. Nat. Protoc. 3, 59–69.
Tsukui, T., Capdevila, J., Tamura, K., Ruiz-Lozano, P., Rodriguez-Esteban, C., Yonei-Tamura, S., Magallón, J., Chandraratna, R. A., Chien, K., Blumberg, B., et al. (1999). Multiple left-right asymmetry defects in Shh(-/-) mutant mice unveil a convergence of the shh and retinoic acid pathways in the control of Lefty-1. Proc. Natl. Acad. Sci. USA 96, 11376–11381.
Veerkamp, J., Rudolph, F., Cseresnyes, Z., Priller, F., Otten, C., Renz, M., Schaefer, L. and Abdelilah-Seyfried, S. (2013). Unilateral dampening of Bmp activity by nodal generates cardiac left-right asymmetry. Dev. Cell 24, 660–667.
Wang, G., Cadwallader, A. B., Jang, D. S., Tsang, M., Yost, H. J. and Amack, J. D. (2011). The Rho kinase Rock2b establishes anteroposterior asymmetry of the ciliated Kupffer's vesicle in zebrafish. Development 138, 45–54.
Wang, G., Yost, H. J. and Amack, J. D. (2013). Analysis of gene function and visualization of cilia-generated fluid flow in Kupffer's vesicle. J. Vis. Exp.
Yamamoto, M., Mine, N., Mochida, K., Sakai, Y., Saijoh, Y., Meno, C. and Hamada, H. (2003). Nodal signaling induces the midline barrier by activating Nodal expression in the lateral plate. Development 130, 1795–1804.
Yamanaka, H., Moriguchi, T., Masuyama, N., Kusakabe, M., Hanafusa, H., Takada, R., Takada, S. and Nishida, E. (2002). JNK functions in the non-canonical Wnt pathway to regulate convergent extension movements in vertebrates. EMBO Rep. 3, 69–75.
Yamauchi, H., Miyakawa, N., Miyake, A. and Itoh, N. (2009). Fgf4 is required for left-right patterning of visceral organs in zebrafish. Dev. Biol. 332, 177–185.
Yan, Y. T., Gritsman, K., Ding, J., Burdine, R. D., Corrales, J. D., Price, S. M., Talbot, W. S., Schier, A. F. and Shen, M. M. (1999). Conserved requirement for EGF-CFC genes in vertebrate left-right axis formation. Genes Dev. 13, 2527–2537.
Ybot-Gonzalez, P., Savery, D., Gerrelli, D., Signore, M., Mitchell, C. E., Faux, C. H., Greene, N. D. E. and Copp, A. J. (2007). Convergent extension, planar-cell-polarity signalling and initiation of mouse neural tube closure. Development 134, 789–799.
Yelon, D., Horne, S. A. and Stainier, D. Y. (1999). Restricted expression of cardiac myosin genes reveals regulated aspects of heart tube assembly in zebrafish. Dev. Biol. 214, 23–37.

Yin, C., Kikuchi, K., Hochgreb, T., Poss, K. D. and Stainier, D. Y. R. (2010). Hand2 regulates extracellular matrix remodeling essential for gut-looping morphogenesis in zebrafish. Dev. Cell 18, 973–984.
Yuan, S., Zhao, L., Brueckner, M. and Sun, Z. (2015). Intraciliary calcium oscillations initiate vertebrate left-right asymmetry. Curr. Biol. 25, 556–567.

Figures

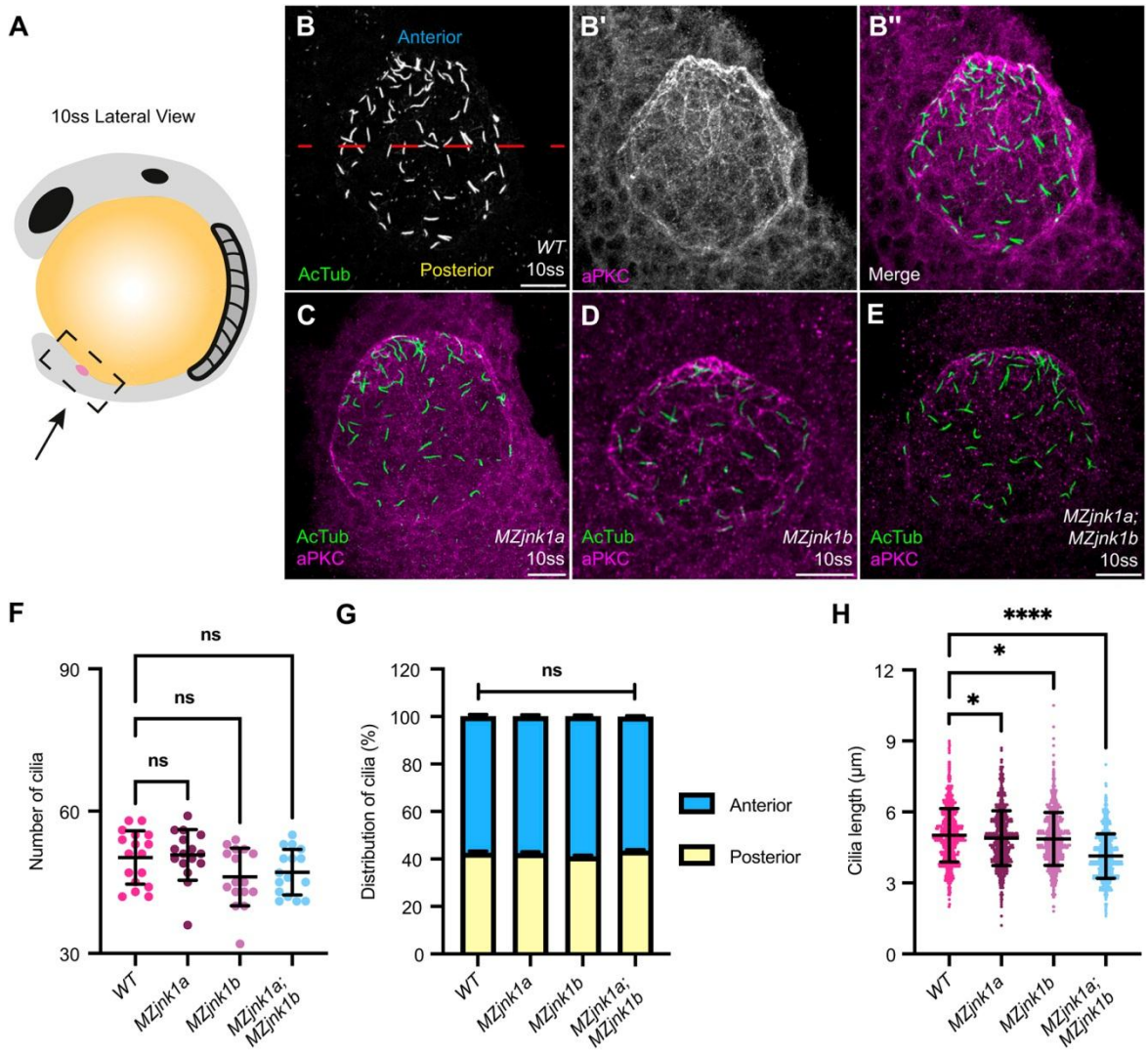

Figure 1. *jnk1a* and *jnk1b* function redundantly to regulate cilia length in the zebrafish left-right organiser

(A) Schematic of zebrafish embryo at 10 somite stage (ss), lateral view. Kupffer's Vesicle (KV, magenta) is located at the caudal tip of the notochord. Box denotes caudal region of embryo imaged in (B-E). **(B-B')** Representative image of WT KV at 10ss used for characterisation of cilial parameters by immunohistochemistry for Acetylated Tubulin with depiction of anterior (blue) and posterior (yellow) in KV (B) and aPKC (B'). **(C-E)** Representative *MZjnk1a* (C) *MZjnk1b* (D) and *MZjnk1a;MZjnk1b* (E) KV at 10ss labelling Acetylated Tubulin (Green) and aPKC (Magenta). **(F)** Quantification of number of cilia in KV of WT, *MZjnk1a, MZjnk1b* and *MZjnk1a;MZjnk1b* embryos at 10ss. *jnk1* mutants display no differences in number of nodal cilia in KV **(G)** Quantification of nodal cilia distribution of in WT, *MZjnk1a, MZjnk1b* and *MZjnk1a;MZjnk1b* embryos at 10ss. Antero-posterior distribution of nodal cilia is unaffected in *jnk1* mutants. **(H)** Quantification of length of nodal cilial in WT,

MZjnk1a, MZjnk1b and *MZjnk1a;MZjnk1b* embryos at 10ss. *MZjnk1a* and *MZjnk1b* mutant embryos display a similar, significant reduction in cilia length. Loss of both *jnk1a* and results in a more dramatic reduction in cilia length. F: Mean ± S.D, One-way ANOVA, multiple comparisons, WT n=17, *MZjnk1a*, *MZjnk1b* and *MZjnk1a;MZjnk1b* n=16. G: Mean ± S.E.M, Two-way ANOVA, multiple comparisons, n=16. H: Mean ± S.D, One-way ANOVA, multiple comparisons, WT n=809, *MZjnk1a* n=812, *MZjnk1b* n=743, *MZjnk1a:MZjnk1b* n=754. ns: not significant, *: $p<0.05$, ****: $p<0.0001$. B-E, Anterior up, left: left. Scale bar: 20µm.

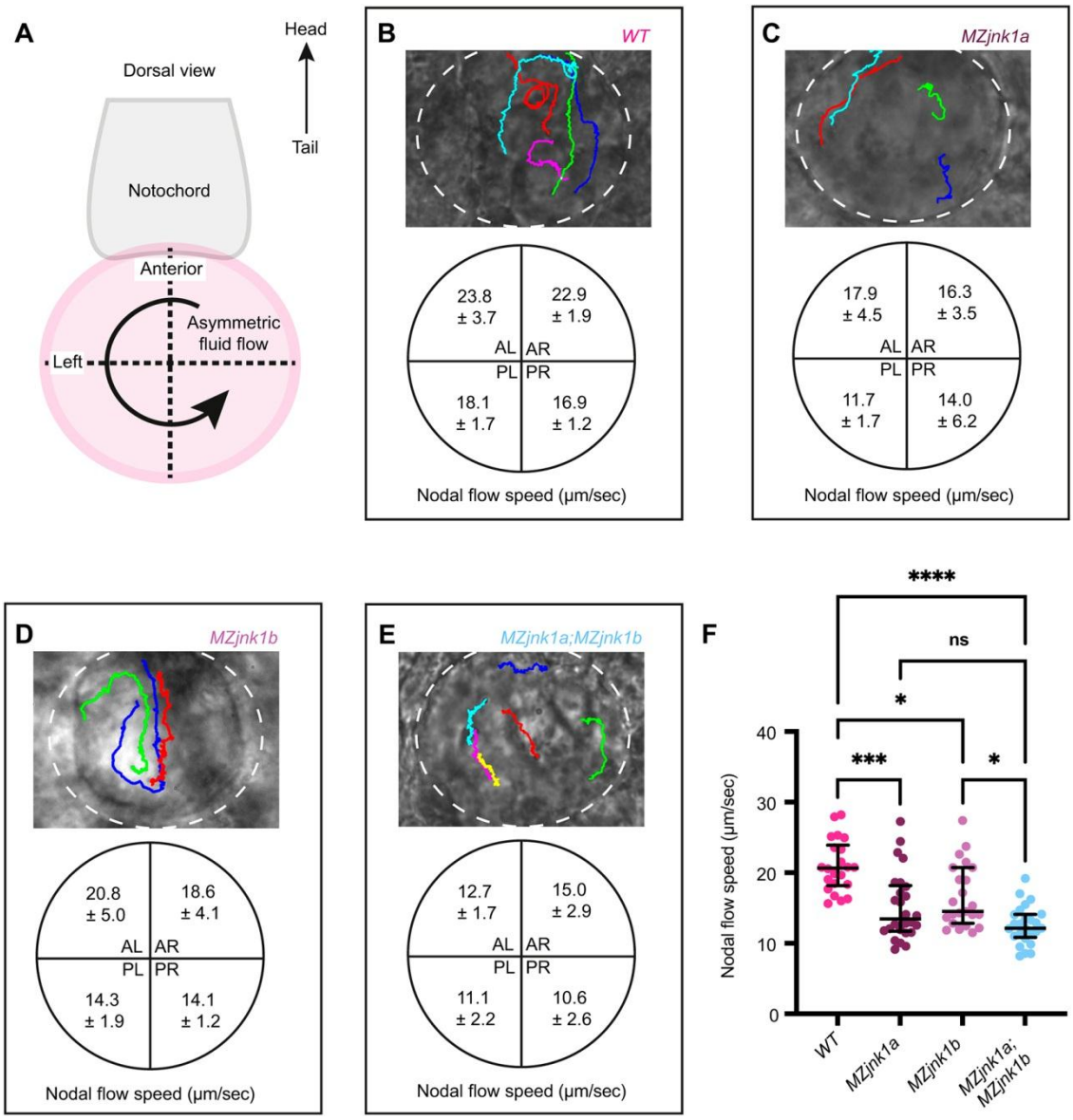

Figure 2. *jnk1a* and *jnk1b* are required for fluid flow in KV

(A) Schematic showing KV (magenta) at the base of the notochord (grey) and direction of nodal flow (arrow) at 10-14ss. The notochord was used to define the antero-posterior and left-right axes for subdivision of KV into quadrants. **(B-E)** Representative brightfield image of WT (B), *MZjnk1a* (C), *MZjnk1b* (D) and *MZjnk1a;MZjnk1b* KV (white dotted line) and traces of bead trajectories over time (coloured lines), together with mean bead speed (µm/s) in each quadrant ± S.D. **(F)** Quantification of average bead speed in KV between 10-14ss. *MZjnk1a* and *MZjnk1b* mutant embryos have significantly slower average nodal flow compared to WT controls. Loss of both *jnk1a* and *jnk1b* results in a greater reduction in average speed. F: Median ± Interquartile Range, Kruskal-Wallis test, multiple comparisons, WT n=22 beads across 6 embryos, *MZjnk1a* n=26 beads across 4 embryos, *MZjnk1b* n=23 beads across 3 embryos, *MZjnk1a;MZjnk1b* n=25 beads across 4 embryos. B-E: Anterior up, left: left. ns: not significant *: p<0.05, ***: p<0.001, ****: p<0.0001. AL: anterior left, AR: anterior right, PL: posterior left, PR: posterior right.

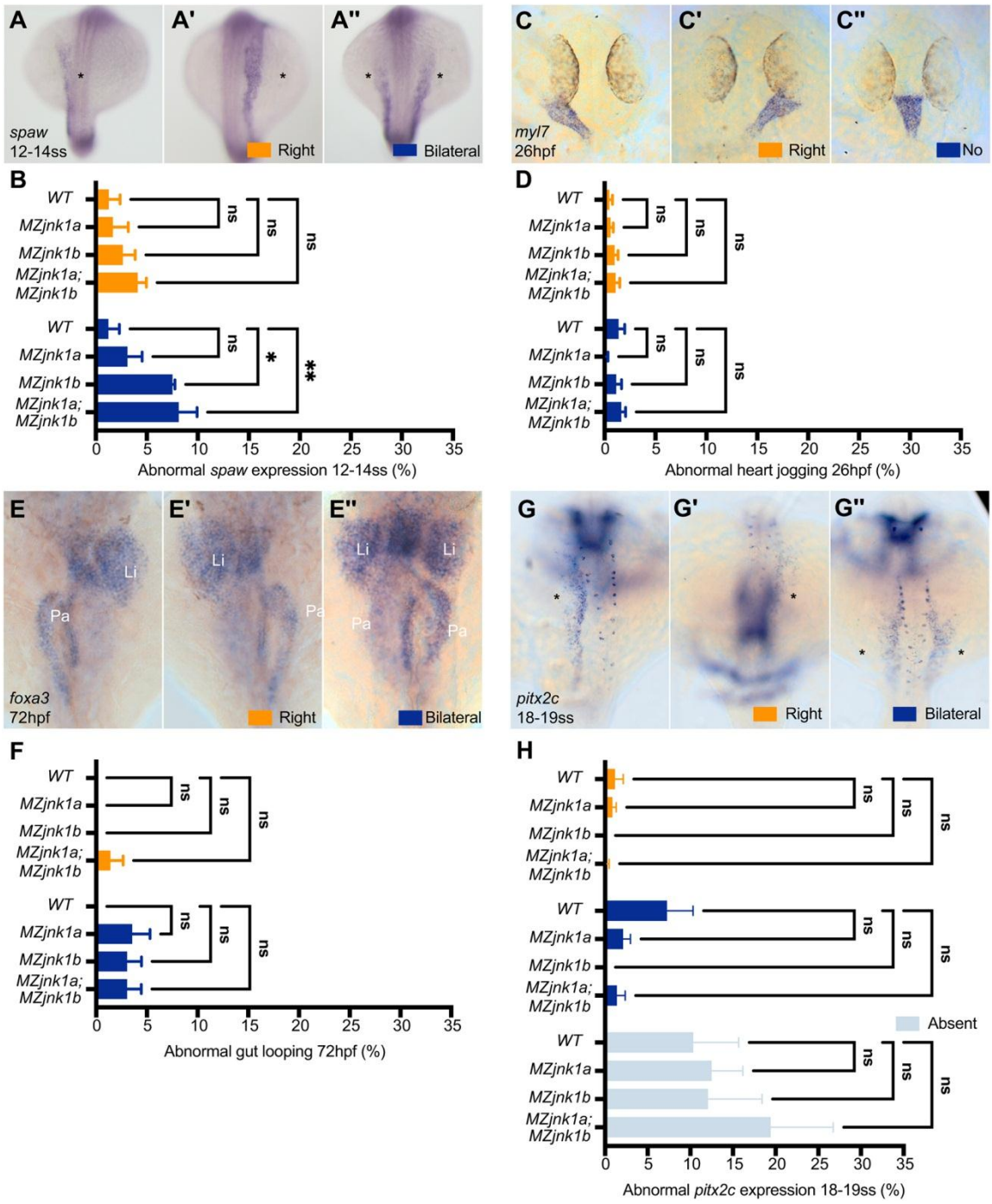

Figure 3. Loss of *jnk1* disrupts Nodal signalling, but not organ asymmetry

(A-A'') Representative images of mRNA *in situ* hybridisation for the zebrafish *Nodal* homolog *southpaw* (*spaw*) at 12-14ss, showing normal expression in the left lateral plate mesoderm (LPM) (A, asterisk), abnormal right-sided (A', asterisk) or bilateral expression (A'', asterisks). **(B)** Characterisation of abnormal *spaw* expression in WT, *MZjnk1a*, *MZjnk1b* and *MZjnk1a;MZjnk1b* mutants at 12-14ss. *MZjnk1b* and *MZjnk1a;MZjnk1b* mutants display a significant increase in the percentage of embryos with bilateral *spaw* expression. Loss of *jnk1a* alone does not have a significant impact on *spaw* expression. **(C-C'')** Representative images of mRNA *in situ* hybridisation of the pan-cardiac marker *myosin, light chain 7,*

regulatory (*myl7)* at 26hpf showing normal left jogging of the heart (C), abnormal right jogging (C') or no jogging (C''). **(D)** Quantification of jogging in WT, *MZjnk1a*, *MZjnk1b* and *MZjnk1a;MZjnk1b* mutants at 26hpf. Loss of *jnk1* does not affect heart jogging. **(E-E'')** Representative images of mRNA *in situ* hybridisation of the endodermal marker *forkhead box A3 (foxa3)* at 72hpf showing organ placement of the Liver (Li) and Pancreas (Pa) following gut looping (E), reversed gut looping (E') or a failure of LPM migration, resulting in a bilateral gut, most obviously observed by the presence of bilaterally positioned Livers (E''). **(F)** Quantification of gut looping in WT, *MZjnk1a*, *MZjnk1b* and *MZjnk1a;MZjnk1b* mutants at 72hpf. Loss of *jnk1* does not affect endoderm morphogenesis. **(G-G'')** Representative images of mRNA *in situ* hybridisation of *paired-liked homeodomain 2, isoform c (pitx2c)* at 18-19ss, showing normal in the left lateral plate mesoderm (F, asterisk), abnormal right-sided (F', asterisk) or bilateral expression (F'', asterisks). **(H)** Characterisation of abnormal *pitx2c* expression in WT, *MZjnk1a*, *MZjnk1b* and *MZjnk1a;MZjnk1b* mutants at 18-19ss. Loss of *jnk1* does not result in abnormal expression of *pitx2c*. B: Mean ± S.E.M, Two-way ANOVA comparison of Right and Bilateral. N=3 clutches, minimum clutch size WT, n=27, *MZjnk1a*, n=21, *MZjnk1b*, n=27, *MZjnk1a*;*MZjnk1b*, n=17. D: Mean ± S.E.M, Two-way ANOVA comparison of Right and No jog. N=7 clutches for WT, N=6 clutches for *MZjnk1a*, N=8 clutches for *MZjnk1b* and *MZjnk1a;MZjnk1b*. Minimum clutch size WT, n=32, *MZjnk1a*, n =46, *MZjnk1b*, n=46, *MZjnk1a: MZjnk1b*, n=43. F: Mean ± S.E.M, Two-way ANOVA comparison of Right and Bilateral. N=3 clutches, minimum clutch size WT, n=25, *MZjnk1a* n=16, *MZjnk1b* n=21, *MZjnk1a;MZjnk1b* n=22. H: Mean ± S.E.M, Two-way ANOVA, multiple comparisons analysing Right, Bilateral and Absent. N=5 clutches, minimum clutch size WT, n=75, *MZjnk1a*, n =73, *MZjnk1b*, n=64, *MZjnk1a:MZjnk1b*, n=37. A-A'', C-C'', G-G'': Dorsal view, E-E'' Ventral view. ns: not significant, *: $p<0.05$, **: $p<0.01$.

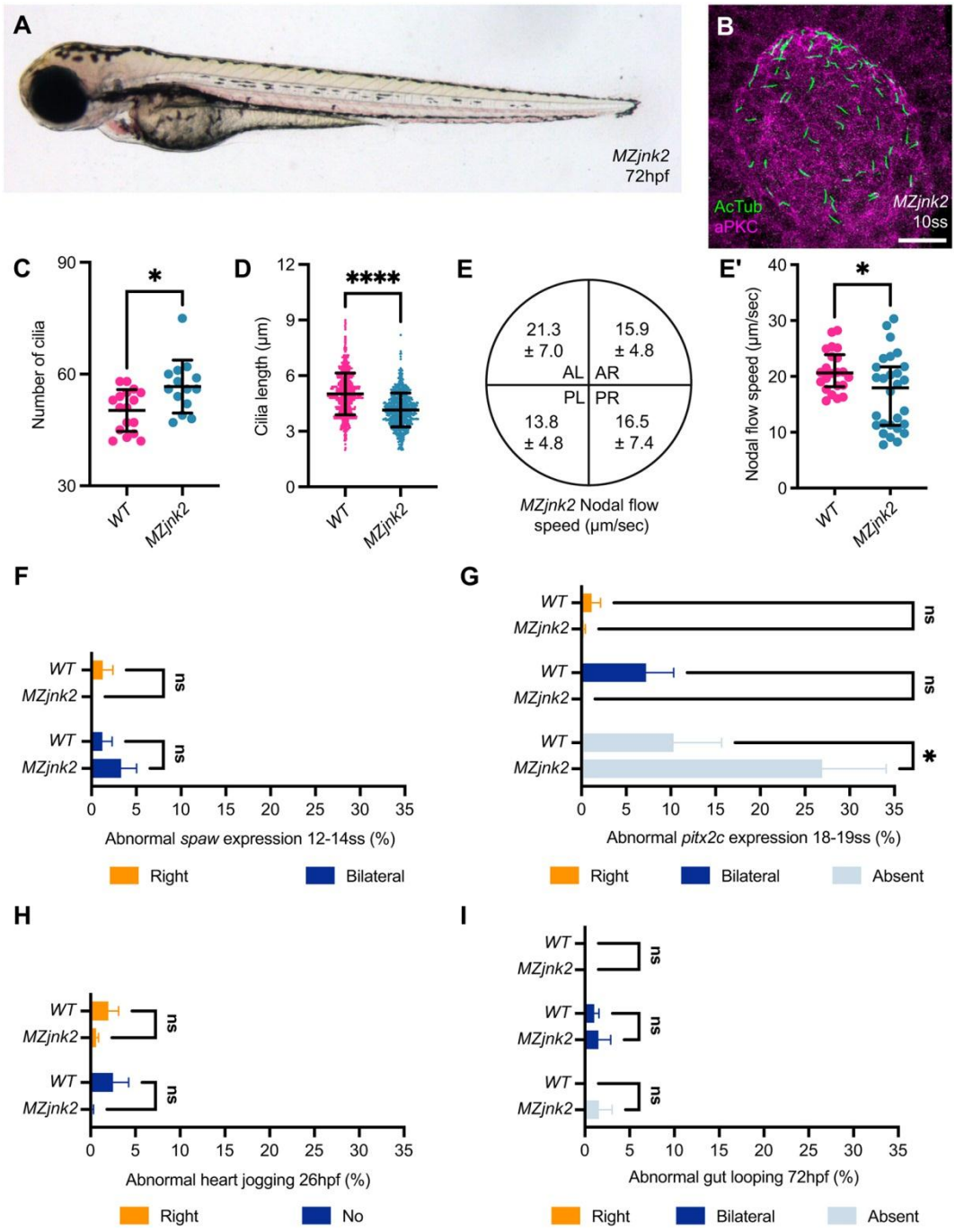

Figure 4. *jnk2* regulates nodal cilia development and KV flow

(A) Representative bright-field image of *MZjnk2* mutant at 3dpf. **(B)** Representative *MZjnk2* KV at 10ss labelling Acetylated Tubulin (Green) and aPKC (Magenta). **(C)** Quantification of number of cilia in WT and *MZjnk2* embryos at 10ss. Loss of *jnk2* results in a significant increase in the number of nodal cilia. **(D)** Quantification of length of nodal cilial in WT and *MZjnk2* embryos at 10ss. *MZjnk2* mutant embryos have a significant reduction in the length of nodal cilia. **(E-E')** Quantification of nodal flow speed in *MZjnk2* by quadrant (µm/s), Mean ± S.D (E) and average speed (E') between 10-14ss. Loss of *jnk2* results in a significant reduction in average speed (E'). **(F)** Loss of *jnk2* does not impact normal *spaw* expression at 12-14ss. **(G)** Characterisation of abnormal *pitx2c* expression in WT and *MZjnk2* mutants at

18-19ss. Loss of *jnk2* results in a significant proportion of embryos which do not have *pitx2c* expression in the lateral plate mesoderm. **(H)** Heart jogging is unaffected in *MZjnk2* mutants. **(I)** Gut looping occurs normally in *MZjnk2* mutants. C: Mean ± S.D, Welch's t-test, *MZjnk2* n=14, WT from Figure 1F. D: Mean ± S.D, Welch's t-test, *MZjnk2* n=737, WT from Figure 1H. E': Median ± Interquartile Range, Mann-Whitney test, *MZjnk2* n=28 beads cross 6 embryos, WT from Figure 2F. F: Mean ± S.E.M, Two-way ANOVA comparison of Right and Bilateral. N=3 clutches, minimum clutch size *MZjnk2*, n=24. WT from Figure 3B. G: Mean ± S.E.M, Two-way ANOVA, multiple comparisons analysing Right, Bilateral and Absent. N=5 clutches, minimum clutch size *MZjnk2*, n=81, WT from Figure 3H. H: Mean ± S.E.M, Two-way ANOVA comparison of Right and No jog. N=6 clutches for WT and *MZjnk2*. Minimum clutch size WT, n=101 and *MZjnk2*, n=46. I: Mean ± S.E.M, Two-way ANOVA comparison of Right and Bilateral. N=3 clutches, minimum clutch size WT, n=98, *MZjnk2*, n=89. A: lateral view, anterior left, B: anterior up. Scale bar: 20µm. ns: not significant, *: $p<0.05$, ****: $p<0.0001$. AL: anterior left, AR: anterior right, PL: posterior left, PR: posterior right.

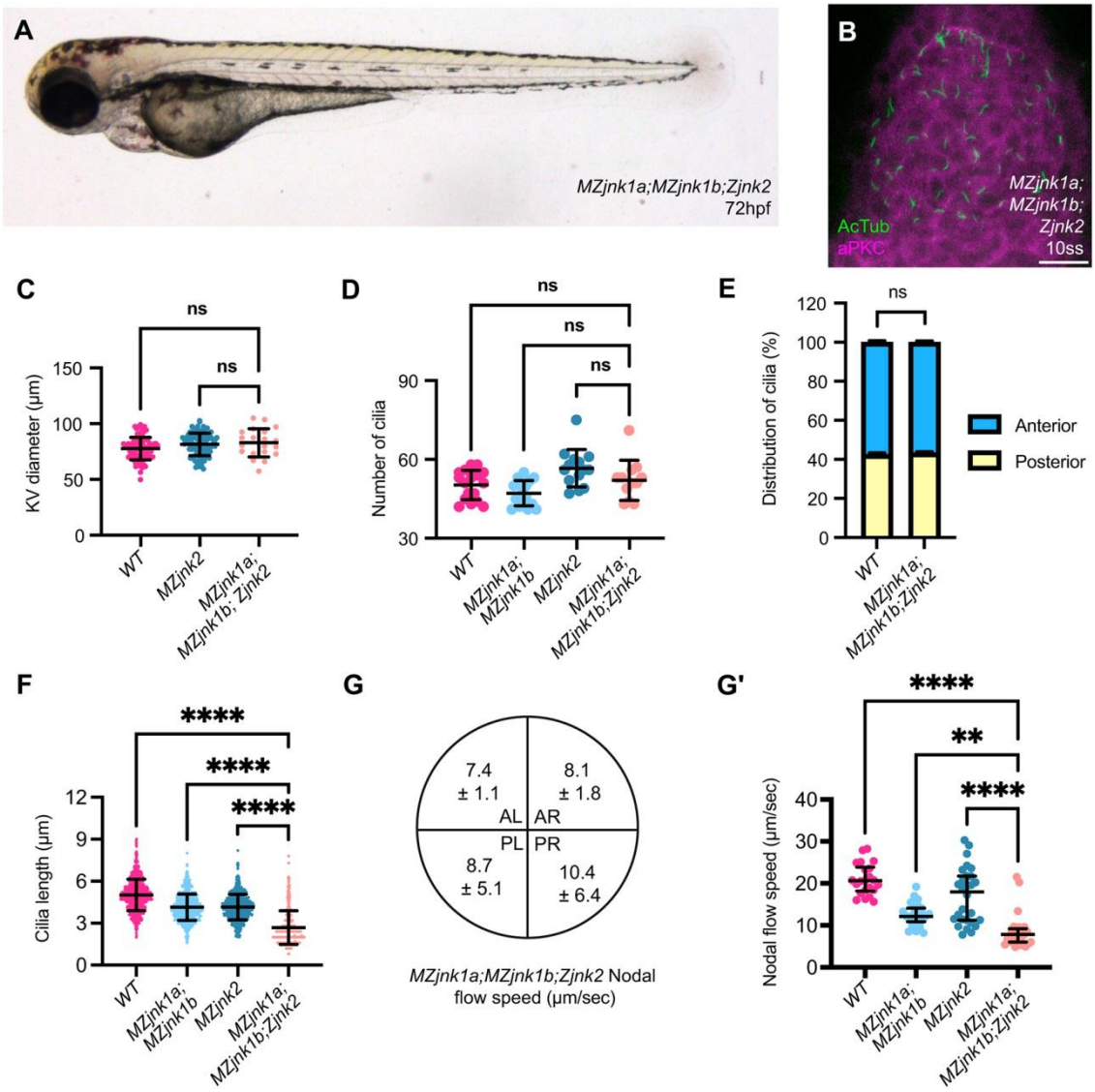

Figure 5. *jnk1a, jnk1b* and *jnk2* function together in nodal cilia development and KV function

(A) Representative bright-field image of *MZjnk1a;MZjnk1b;Zjnk2* embryo at 3dpf. **(B)** Representative *MZjnk1a;MZjnk1b;Zjnk2* KV at 10ss labelling Acetylated Tubulin (Green) and aPKC (Magenta). **(C)** KV diameter quantification in WT, *MZjnk2* and *MZjnk1a;MZjnk1b;Zjnk2* mutant embryos at 8ss. KV size is not impacted by loss of *jnk1* and *jnk2* function. **(D)** Quantification of number of cilia in WT, *MZjnk1a;MZjnk1b*, *MZjnk2* and *MZjnk1a;MZjnk1b;Zjnk2* mutant embryos at 10ss. Loss of *jnk1a*, *jnk1b* and *jnk2* does not impact cilia number in KV. **(E)** Quantification of nodal cilia distribution in WT and *MZjnk1a;MZjnk1b;Zjnk2* embryos at 10ss. Antero-posterior distribution of nodal cilia is unaffected by loss of *jnk2* in a *jnk1* null background. **(F)** Quantification of length of nodal cilial in WT, *MZjnk1a;MZjnk1b*, *MZjnk2* and *MZjnk1a;MZjnk1b;Zjnk2* mutant embryos at 10ss. *MZjnk1a;MZjnk1b;Zjnk2* mutant embryos have a greater reduction in the length of nodal cilia compared to *MZjnk1a;MZjnk1b* or *MZjnk2* mutants. **(G-G')** Quantification of nodal flow speed

in *MZjnk1a;MZjnk1b;Zjnk2* by quadrant (µm/s), Mean ± S.D (G) and average speed (G') between 10-14ss. *MZjnk1a;MZjnk1b;Zjnk2* mutant embryos have a greater reduction in the average speed of nodal flow compared to *MZjnk1a;MZjnk1b* or *MZjnk2* mutants. C: Mean ± S.D, One-way ANOVA, multiple comparisons, *MZjnk1a;MZjnk1b;Zjnk2* n=20, WT from Figure S1B, *MZjnk2* from Figure S2C. D: Mean ± S.D, One-way ANOVA, multiple comparisons, *MZjnk1a;MZjnk1b;Zjnk2* n=12, WT and *MZjnk1a:MZjnk1b* from Figure 1F, *MZjnk2* from Figure 4C. E: Mean ± S.E.M, Two-way ANOVA, multiple comparisons, *MZjnk1a;MZjnk1b;Zjnk2* n=14, WT from Figure 1G. F: Mean ± S.D, One-way ANOVA, multiple comparisons, *MZjnk1a;MZjnk1b;Zjnk2* n=466, WT and *MZjnk1a:MZjnk1b* from Figure 1H, *MZjnk2* from Figure 4D. G': Median ± Interquartile range, Kruskal-Wallis test, multiple comparisons, *MZjnk1a;MZjnk1b;Zjnk2* n=28 beads across 3 embryos, WT and *MZjnk1a:MZjnk1b* from Figure 2F, *MZjnk2* from Figure 4E'. A: Lateral view, anterior left. B: anterior up. Scale bar: 20µm. ns: not significant, **: $p<0.01$, ****: $p<0.0001$. AL: anterior left, AR: anterior right, PL: posterior left, PR: posterior right.

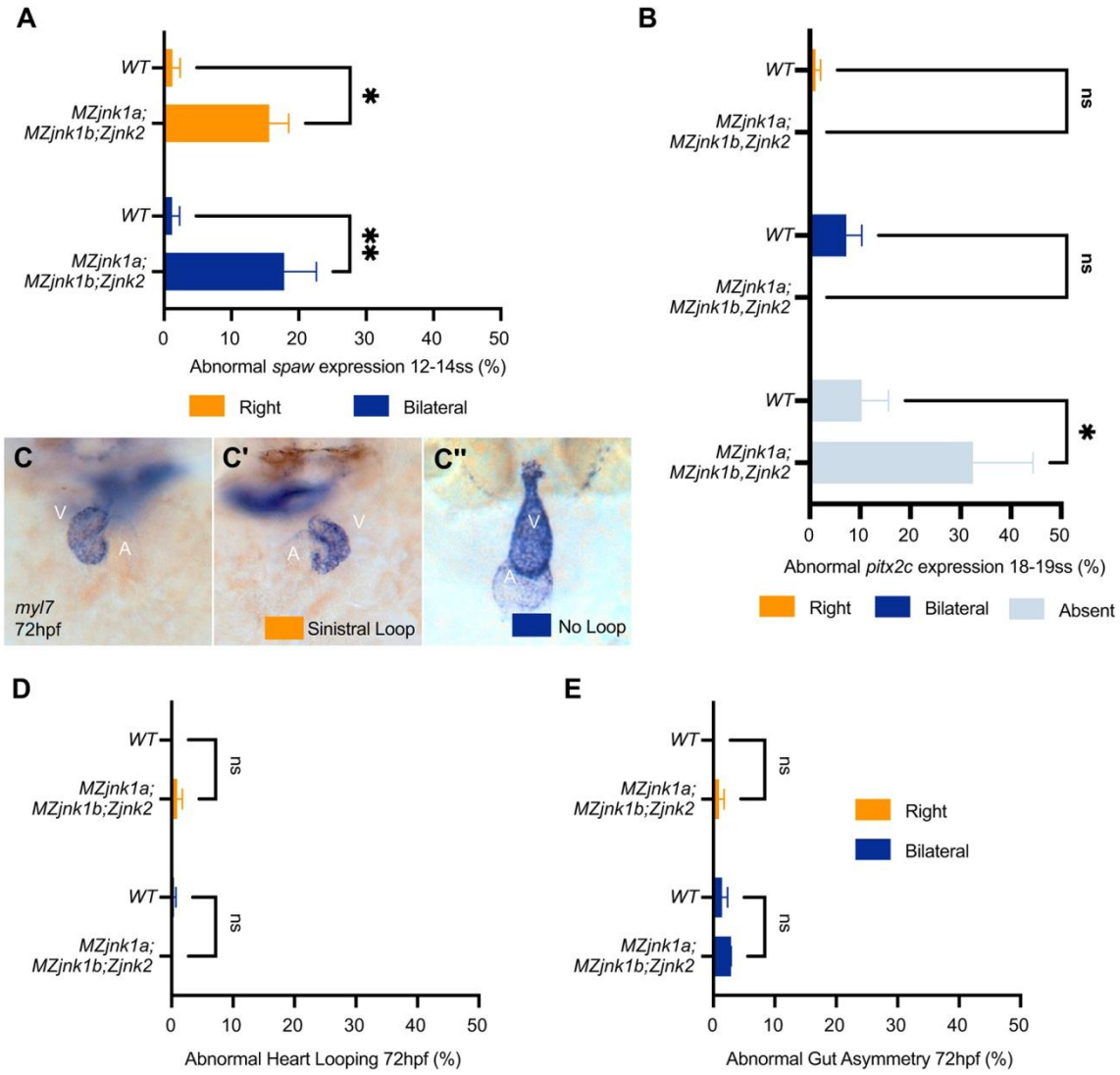

Figure 6. Asymmetric *spaw* expression is dispensable for organ asymmetry

(A) Characterisation of abnormal *spaw* expression in WT and *MZjnk1a;MZjnk1b;Zjnk2* mutants at 12-14ss. Loss of *jnk1* and *jnk2* results in approximately 40% of embryos displaying either right or bilateral *spaw* expression. **(B)** Characterisation of abnormal *pitx2c* expression in WT and *MZjnk1a;MZjnk1b;Zjnk2* mutants at 18-19ss, loss of *jnk1* and *jnk2* results in a significant increase in the proportion of embryos without *pitx2c* expression in the LPM. **(C-C'')** Representative images of mRNA *in situ* hybridisation of the pan-cardiac marker *myl7* at 72hpf showing normal dextral looping of the heart (C), abnormal sinistral (reverse) looping (C') or non-looped hearts (C''). Quantification of **(D)** heart looping and **(E)** gut looping in WT and *MZjnk1a;MZjnk1b;Zjnk2* mutants at 72hpf. Loss of *jnk1* and *jnk2* activity does not impact organ laterality. A: Mean ± S.E.M, Two-way ANOVA comparison of Right and Bilateral. N=3 clutches, minimum clutch size *MZjnk1a;MZjnk1b;Zjnk2*, n=10. WT from Figure 3B. B: Mean ± S.E.M, Two-way ANOVA, multiple comparisons analysing Right, Bilateral and Absent. N=5 clutches, minimum clutch size *MZjnk1a;MZjnk1b;Zjnk2*, n=40 WT from Figure

3H. D: Mean ± S.E.M, Two-way ANOVA comparison of sinistral and no loop. N=3 clutches. Minimum clutch size WT, n=88, *MZjnk1a;MZjnk1b;Zjnk2*, n=34. E: Mean ± S.E.M, Two-way ANOVA comparison of Right and Bilateral. N=3 clutches, same clutches as 6D. C-C''; Ventral view. ns: not significant, *: p<0.05, **: p<0.01. V: ventricle, A: atrium.

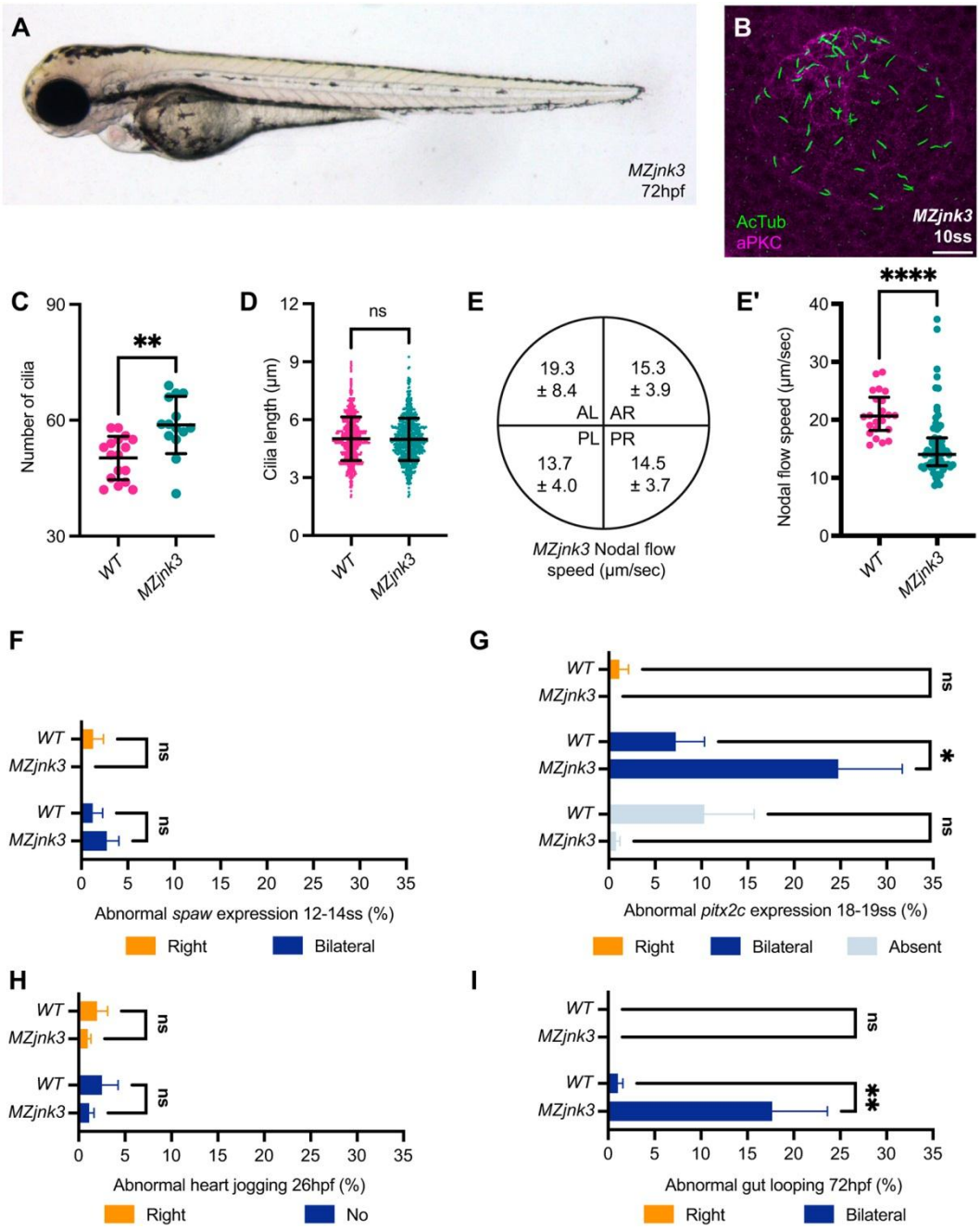

Figure 7. *jnk3* is required to restrict *pitx2c*

(A) Representative bright-field image of *MZjnk3* mutant at 3dpf. **(B)** Representative *MZjnk3* KV at 10ss labelling Acetylated Tubulin (Green) and aPKC (Magenta). **(C)** Quantification of number of cilia in WT and *MZjnk3* embryos at 10ss. Loss of *jnk3* results in a significant increase in the number of nodal cilia. **(D)** Quantification of length of nodal cilial in WT and *MZjnk3* embryos at 10ss. Loss of *jnk3* does not affect cilial length. **(E-E')** Quantification of nodal flow speed in *MZjnk3* by quadrant (µm/s), Mean ± S.D (E) and average speed (E') between 10-14ss. Loss of *jnk3* results in a significant reduction in average speed (E'). **(F)** Loss of *jnk3* does not impact normal *spaw* expression at 12-14ss. **(G)** Characterisation of abnormal *pitx2c* expression in WT and *MZjnk3* mutants at 18-19ss. Loss of *jnk3* leads to a

significant increase in the proportion of embryos which display bilateral *pitx2c* expression. **(H)** Heart jogging is unaffected in *MZjnk3* mutants. **(I)** *MZjnk3* mutants have a significant proportion of bilaterally positioned abdominal organs. C: Mean ± S.D, Welch's t test, *MZjnk3* n=14, WT from Figure 1F. D: Mean ± S.D, Welch's t test, *MZjnk3* n=720, WT from Figure 1H. E': Median ± Interquartile Range, Mann-Whitney test, *MZjnk3* n=61 beads across 11 embryos, WT from Figure 2F. F: Mean ± S.E.M, Two-way ANOVA comparison of Right and Bilateral. N=3 clutches, minimum clutch size *MZjnk3* n=23. WT from Figure 3B. G: Mean ± S.E.M, Two-way ANOVA, multiple comparisons analysing Right, Bilateral and Absent. N=5 clutches, minimum clutch size *MZjnk3* n=81, WT from Figure 3H. H: Mean ± S.E.M, Two-way ANOVA comparison of Right and No jog. N=8 clutches for *MZjnk3*, Minimum clutch *MZjnk3*, n=46, WT from Figure 4H. I: Mean ± S.E.M, Two-way ANOVA comparison of Right and Bilateral. N=3 clutches, minimum clutch size *MZjnk3*, n=92, WT from Figure 4I. A: lateral view, anterior left, B: anterior up. Scale bar: 20μm. ns: not significant, *: $p<0.05$, **:$p<0.01$, ****: $p<0.0001$. AL: anterior left, AR: anterior right, PL: posterior left, PR: posterior right.

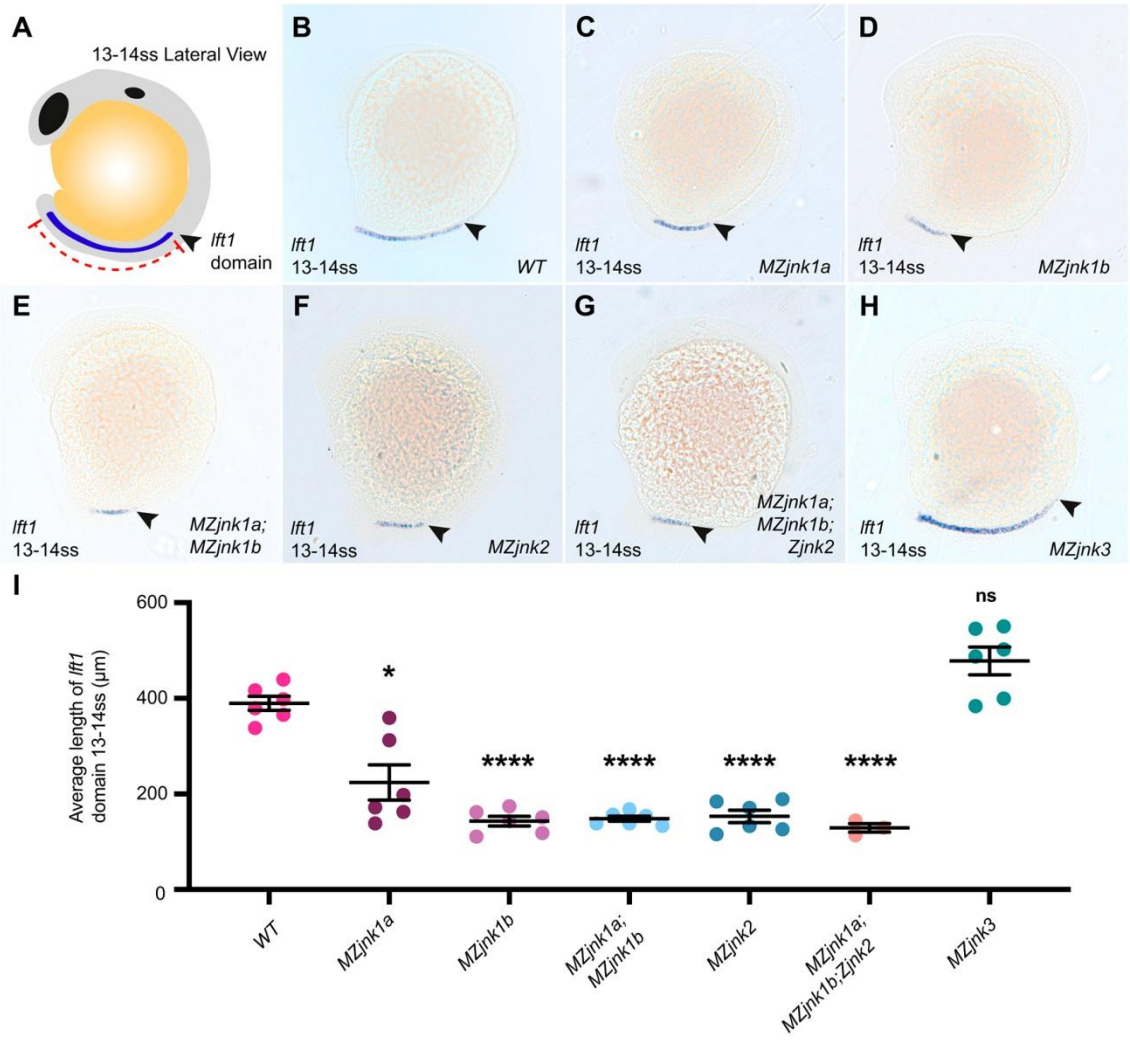

Figure 8. *jnk1* and *jnk2* are required for early establishment of the midline barrier

(A) Schematic of zebrafish embryo at 1314ss, lateral view. *lefty1* (*lft1)* expression (blue) extends anteriorly from the base of the notochord (red). Arrowhead marks anterior limit of expression. Representative images of mRNA *in situ* hybridisation of *lft1* at 13-14ss in **(B)** WT, **(C)** *MZjnk1a*, **(D)** *MZjnk1b*, **(E)** *MZjnk1a;MZjnk1b*, **(F)** *MZjnk2*, **(G)** *MZjnk1a;MZjnk1b;Zjnk2* and **(H)** *MZjnk3* mutant embryos. Arrow heads denote anterior limit of *lft1* expression in the notochord. **(I)** Quantification of average length of *lft1* expression at 13-14ss. Loss of *jnk1a* results in ~50% reduction in average length of *lft1* domain. *MZjnk1b*, *MZjnk1a;MZjnk1b*, *MZjnk2* and *MZjnk1a:MZjnk1b;Zjnk2* mutants display a more dramatic and similar reduction in the extent of *lft1* propagation in the notochord. *lft1* expression is unaffected in *MZjnk3* mutants. B-H: lateral view, anterior top. I: Mean ± S.E.M, Brown-Forsythe and Welch ANOVA, multiple comparisons, with notations denoting result of test between WT respective mutant. N=6 clutches, minimum clutch size WT n=82, *MZjnk1a* n=73, *MZjnk1b* n=61, *MZjnk1a*;*MZjnk1b* n=78, *MZjnk2* n=59, *MZjnk3*, n=69 *MZjnk1a;MZjnk1b;Zjnk2,* N=3, minimum clutch size n=37. B-H: lateral view, anterior left. ns: not significant, *: p<0.05, ****: p<0.0001.

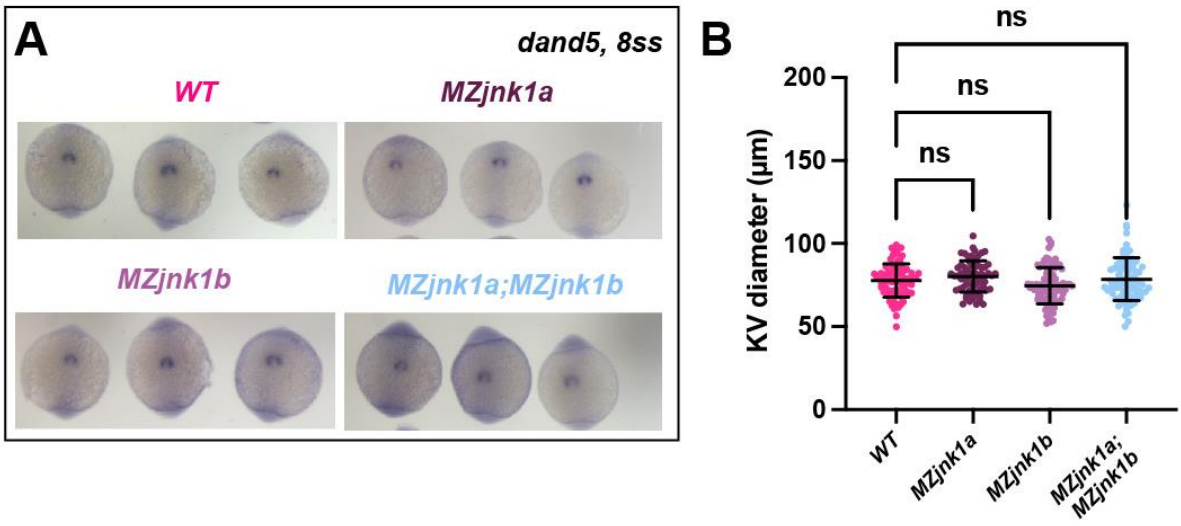

Fig. S1. Loss of *jnk1* does not impact Kupffer's Vesicle Size (A) Representative images of mRNA *in situ* hybridisation of *DAN domain family member 5* (*dand5)* at 8ss marking KV for quantification of diameter in WT, *MZjnk1a, MZjnk1b* and *MZjnk1a;MZjnk1b* embryos. **(B)** KV diameter quantification in WT, *MZjnk1a, MZjnk1b* and *MZjnk1a;MZjnk1b* embryos. KV size is not impacted by loss of *jnk1* function B: Mean ± S.D, One-way ANOVA, multiple comparisons, WT n=94, *MZjnk1a* n=68, *MZjnk1b* n=91, *MZjnk1a;MZjnk1b* n=84. A: Posterior up, left: right.

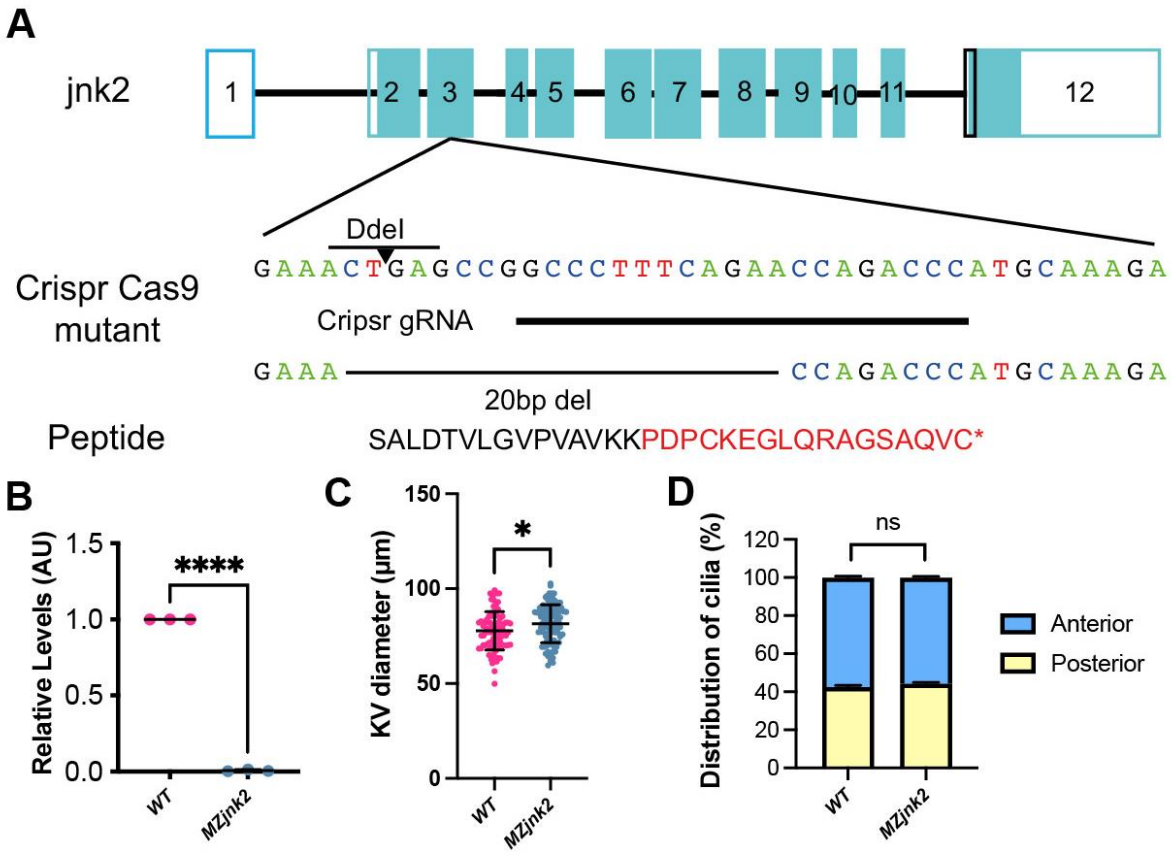

Fig. S2. Generation of *jnk2* mutants by CRISPR-Cas9 genome editing

(A) Schematic of *jnk2* (*mapk9*) gene structure based on ZDB-GENE-091117-28, white denotes untranslated region, green denotes coding sequence. *jnk2* mutants were generated using a single gRNA targeting Exon 3 (ENSDART00000112550.3, isoform 1), downstream of a DdeI restriction enzyme site. The recovered 20bp mutation destroys the DdeI restriction site, generating a frame shift, leading to 17 amino acids of nonsense and a stop codon (red). **(B)** Semi-quantitative PCR demonstrates that *MZjnk2* mutants are a complete null for *jnk2*. **(C)** KV diameter quantification in WT and *MZjnk2* embryos at 8ss. *MZjnk2* mutant embryos display a mild, yet significant increase in KV diameter. **(D)** Quantification of cilial distribution in WT control and *MZjnk2* embryos at 10ss. Antero-posterior distribution of nodal cilia is unaffected by loss of *jnk2*. B: Mean ± Standard Error Mean, Unpaired t test, n = 3. C: Mean ± S.D, Welch's t-test, *MZjnk2* n=94, WT from Figure S1B. D: Mean ± Standard Error Mean, Two-way ANOVA, *MZjnk2* n=16, WT data reproduced from Figure 1G. ns: not significant, *:p<0.05, ****: p<0.0001.

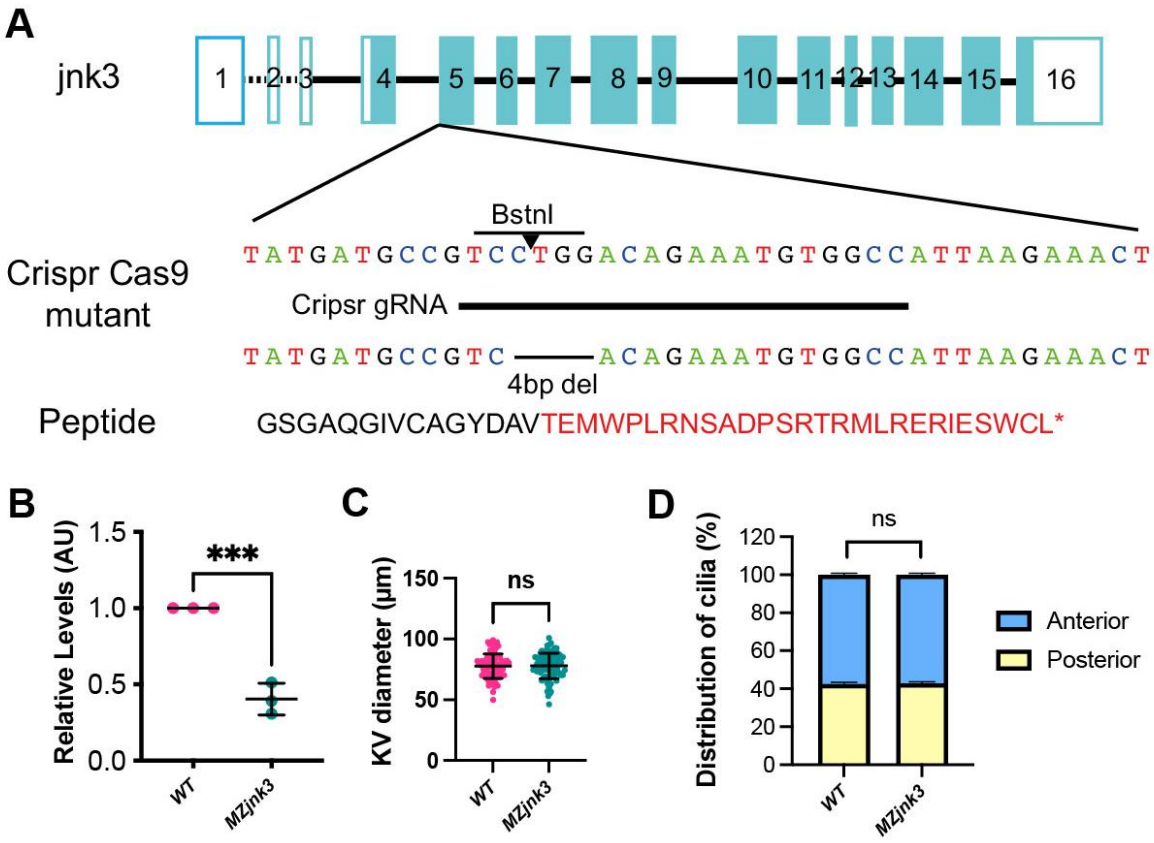

Fig. S3. Generation of *jnk3* mutants by CRISPR-Cas9 genome editing

(A) Schematic of *jnk3* (*mapk10*) gene structure based on ZDB-GENE-051120-117, white denotes UTR, green denotes coding sequence. *jnk3* mutants were generated using a single gRNA targeting Exon 5 (NM_001318318, isoform 1), downstream of a BstnI restriction enzyme site. The recovered 4bp mutation destroys the BstnI restriction site generating a frame shift, leading to 27 amino acids of nonsense and a stop codon (red). **(B)** Semi-quantitative PCR demonstrates that *MZjnk3* mutants have approximately 50% reduction in *jnk3* transcript. **(C)** KV diameter quantification in WT and *MZjnk3* embryos at 8ss. Loss of *jnk3* does not impact KV size. **(D)** Quantification of cilial distribution in WT control and *MZjnk3* embryos at 10ss. Antero-posterior distribution of nodal cilia is unaffected by loss of *jnk3*. B: Mean ± Standard Error Mean, Unpaired t test, n = 3. C: Mean ± S.D, Welch's t test, *MZjnk3* n=89, WT from Figure S1B. D: Mean ± Standard Error Mean, Two-way ANOVA, *MZjnk3* n=16, WT data reproduced from Figure 1G. ns: not significant, ***: p<0.001.

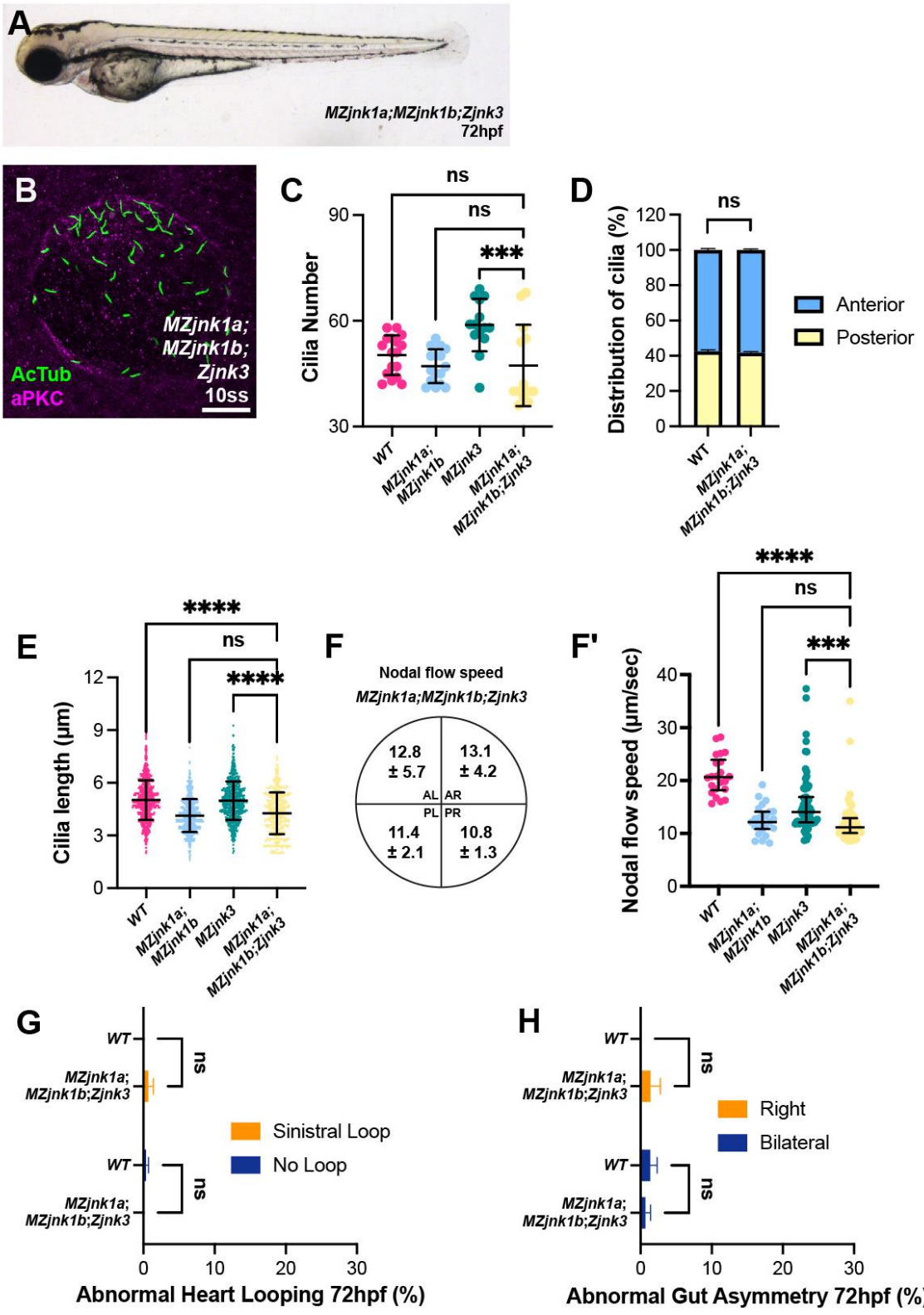

Fig. S4. *jnk3* is epistatic to *jnk1* in generating nodal flow

(A) Representative bright field image of *MZjnk1a;MZjnk1b;Zjnk3* embryo at 3dpf. **(B)** Representative image of *MZjnk1a;MZjnk1b;Zjnk3* KV at 10ss labelling Acetylated Tubulin (Green) and aPKC (Magenta). **(C)** Quantification of number of cilia in WT

control, *MZjnk1a;MZjnk1b*, *MZjnk3* and *MZjnk1a;MZjnk1b;Zjnk3* mutant embryos at 10ss. Loss of *jnk1* activity rescues increased cilia number in *jnk3* mutants. **(D)** Quantification of cilial distribution of in WT control and *MZjnk1a;MZjnk1b;Zjnk3* embryos at 10ss. Antero-posterior distribution of nodal cilia is unaffected by loss of *jnk3* in a *jnk1* null background. **(E)** Quantification of length of nodal cilial in WT control, *MZjnk1a;MZjnk1b*, *MZjnk3* and *MZjnk1a;MZjnk1b;Zjnk3* mutant embryos at 10ss. Loss of *Zjnk3* activity in *MZjnk1a;MZjnk1b* mutant background does not further impact length of nodal cilia. **(F-F')** Quantification of nodal flow speed in *MZjnk1a;MZjnk1b;Zjnk3* by quadrant (F) and average speed (F') between 10-14ss. Loss of *Zjnk3* activity in *MZjnk1a;MZjnk1b* mutant background does not further impact average speed of nodal flow in KV. Quantification of **(G)** heart looping and **(H)** gut looping in WT control and *MZjnk1a;MZjnk1b;Zjnk3* mutants at 72hpf. Loss of *jnk1* and *jnk3* activity does not impact organ laterality. C: Mean ± Standard Deviation, One-way ANOVA with multiple comparisons, *MZjnka1a;MZjnk1b;Zjnk3* n=13, WT and *MZjnk1a;MZjnk1b* data reproduced from Figure 1F, *MZjnk3* data reproduced from Figure 7C. D: Mean ± Standard Error Mean, Two-way ANOVA, *MZjnk1a;MZjnk1b;Zjnk3* n=15, WT data reproduced from Figure 1G. E: Mean ± Standard Deviation, One-way ANOVA with multiple comparisons, *MZjnk1a:MZjnk1b;Zjnk3* n=577, WT and *MZjnk1a:MZjnk1b* data reproduced from Figure 1H, *MZjnk3* data reproduced from Figure 7D. F': Median ± Interquartile Range, Kruskal-Wallis test with multiple comparisons, *MZjnk1a;MZjnk1b;Zjnk3* n = 63 beads across 8 embryos, WT and *MZjnk1a;MZjnk1b* data reproduced from Figure 2F, *MZjnk3* data reproduced from Figure 7E'. G: Mean ± Standard Error Mean, Two-way ANOVA comparison of left and No loop. N = 3 clutches. Minimum clutch size *MZjnk1a;MZjnk1b;Zjnk3*, n = 44, WT data reproduced from 6D. H: Mean ± Standard Error Mean, Two-way ANOVA comparison of Right and Bilateral. N = 3 clutches, same clutches as S4G. WT data reproduced from 6E. A: lateral view, anterior left, B: anterior up. Scale bar: 20μm. ns: not significant, ***: $p<0.001$, ****: $p<0.0001$. AL: anterior left, AR: anterior right, PL: posterior left, PR: posterior right.

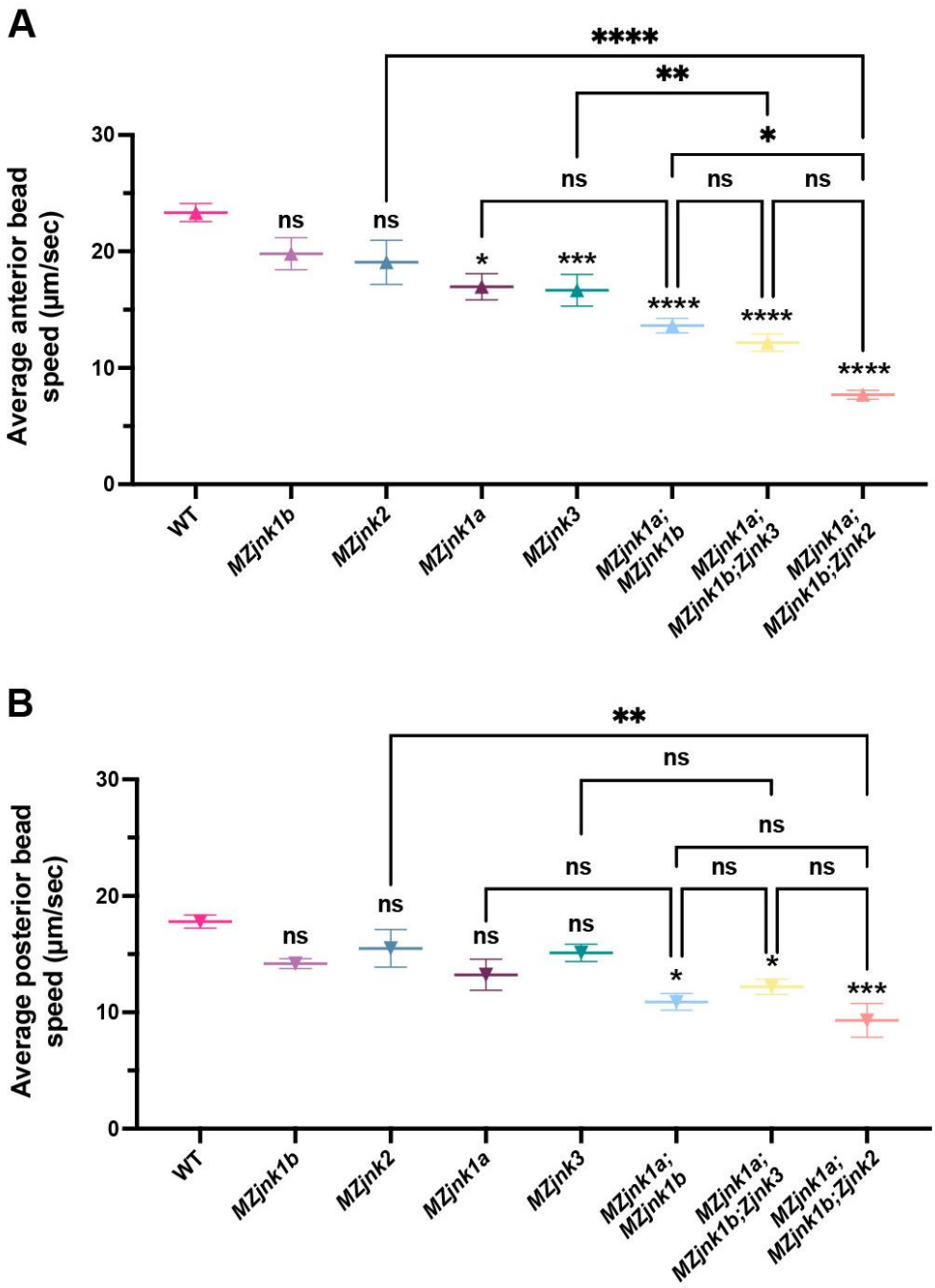

Fig. S5. Loss of *jnk* impacts nodal flow speeds in diverse ways

(A) Average speed of beads imaged in anterior compartment of KV in respective genotype, reproduced from Figures 2, 4, 5, 7 and S4. Notation directly above average values denotes statistical significance when compared to WT. Anterior nodal flow is impacted except in *MZjnk1b* or *MZjnk2* mutants. The most dramatic reduction in anterior nodal flow speed is in *MZjnk1a;MZjnk1b;Zjnk2* mutants. **(B)** Average speed of beads imaged in posterior compartment of KV in respective

genotype, reproduced from Figures 2, 4, 5, 7 and S4. Notation directly above average values denotes statistical significance when compared to WT. Posterior nodal flow is only significantly altered following loss of both *jnk1a* and *jnk1b*, but is not further modified by loss of *jnk2* or *jnk3*. A-B: Mean ± Standard Error Mean, One-way ANOVA with multiple comparisons ns: not significant, *: $p<0.05$, **: $p<0.01$, ***: $p<0.001$, ****: $p<0.0001$.

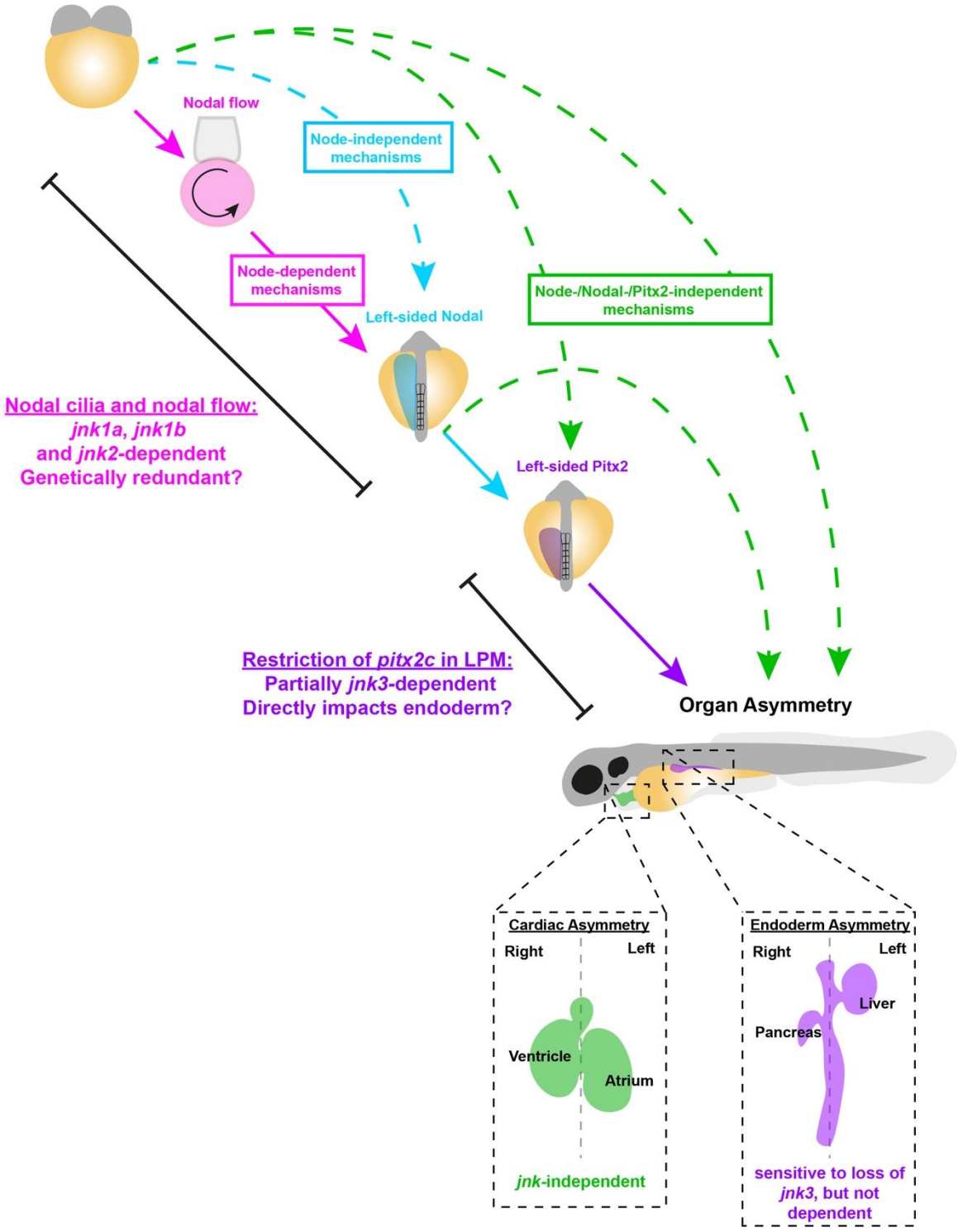

Fig. S6. The role of *jnk* genes in establishment of the left-right axis

Multiple mechanisms ensure robust asymmetric organ placement during development. An early node-dependent mechanism (magenta), requiring both *jnk1* and *jnk2* functions to specify cilia length and drive directional nodal flow. Nodal flow

(magenta) and Node-independent mechanisms (blue) result in asymmetric, left-side restricted *Nodal* (blue) in the left LPM. Downstream of Nodal and other early acting mechanisms, *Pitx2* expression is restricted to the left LPM, which is partially dependent on *jnk3* (purple). Pathways independent of the node, *Nodal* and *Pitx2* function also define the left-right axis in parallel and may act downstream of *Nodal* expression (green). A combination of *Nodal* and *Pitx2*-dependent and -independent pathways result in organ asymmetry. Some organs such as the heart, undergo asymmetric morphogenesis independent of node, *Nodal*, *Pitx2* or *jnk* activity (green) whilst endoderm asymmetry may be dependent on restricted *pitx2c* expression, which partially requires *jnk3* (purple) or function through *Pitx2*-independent, mechanisms which are sensitised to disruption in *MZjnk3* mutants.

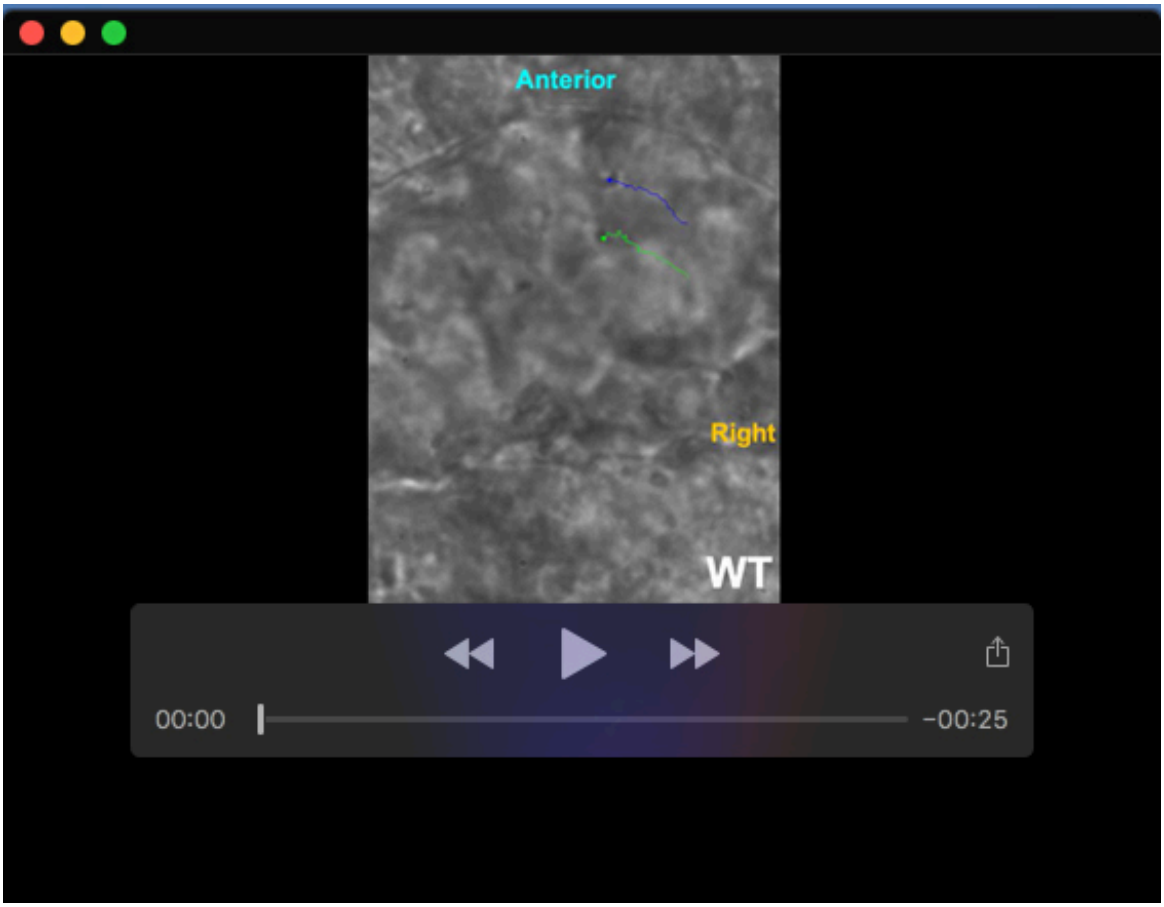

Movie 1. WT Kupffer's Vesicle

Brightfield movie of example WT control Kupffer's vesicle injected with beads for quantification of nodal flow, imaged using a 60X objective. Dark blue and green traces: Representative Anterior, red trace: Representative Posterior.

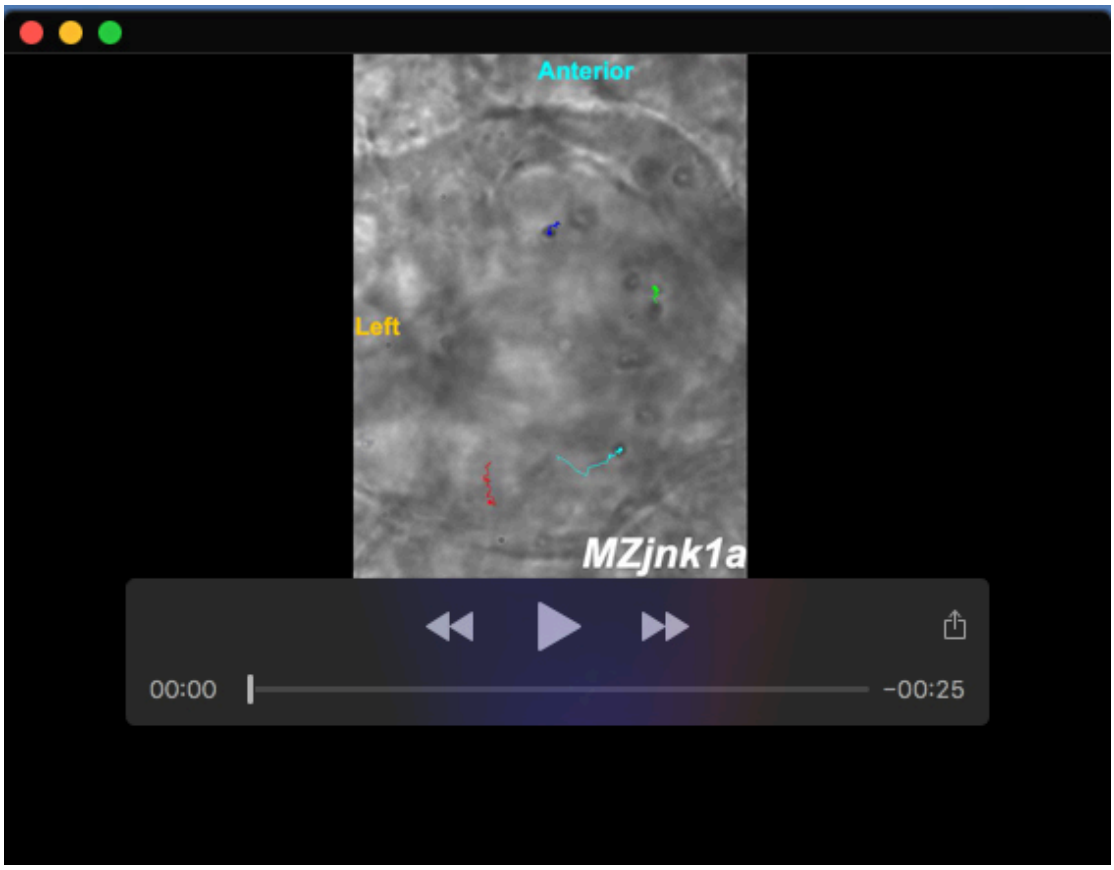

Movie 2. *MZjnk1a* Kupffer's Vesicle

Brightfield movie of example *MZjnk1a* Kupffer's vesicle injected with beads for quantification of nodal flow, imaged using a 60X objective. Dark blue and green traces: Representative Anterior, red and light blue traces: Representative Posterior.

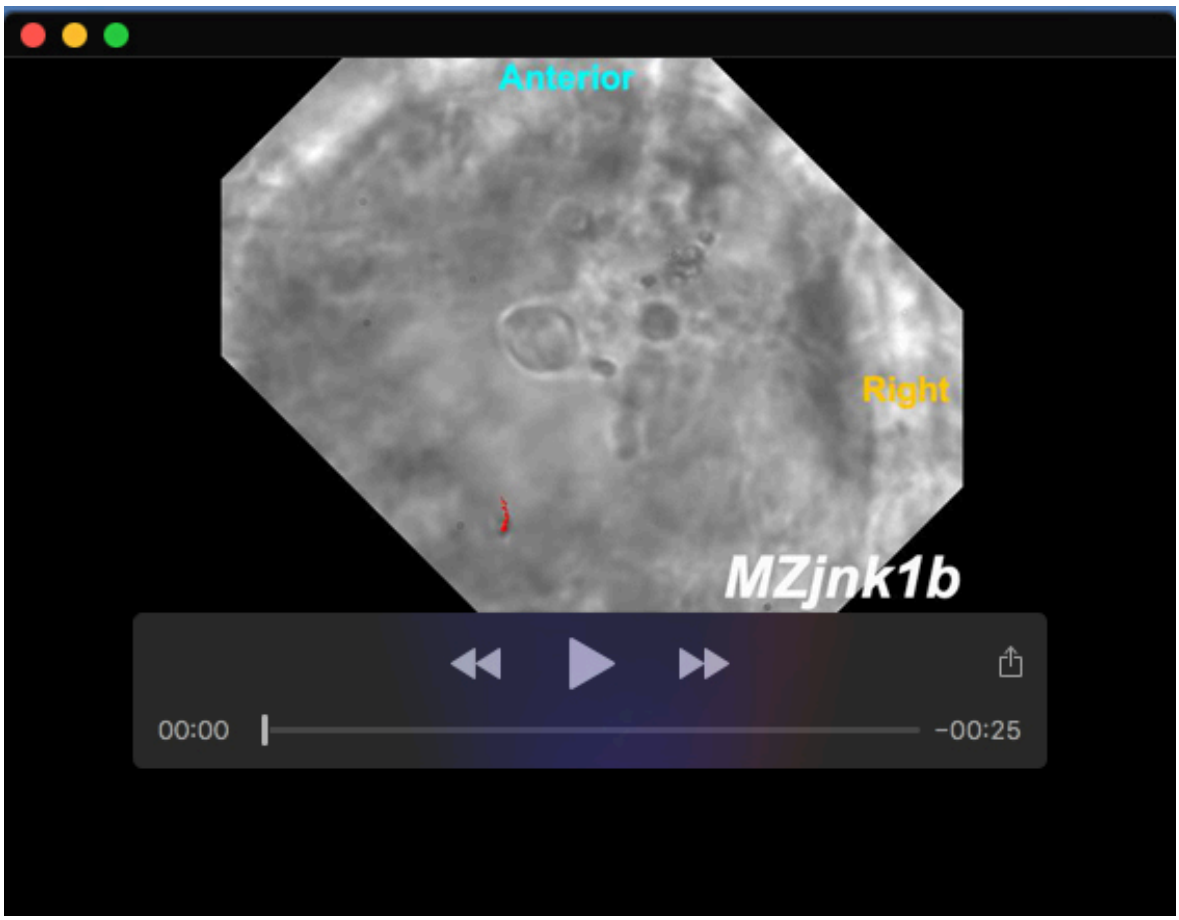

Movie 3. *MZjnk1b* Kupffer's Vesicle

Brightfield movie of example *MZjnk1b* Kupffer's vesicle injected with beads for quantification of nodal flow, imaged using a 60X objective. Dark blue and green traces: Representative Anterior, red and light blue traces: Representative Posterior.

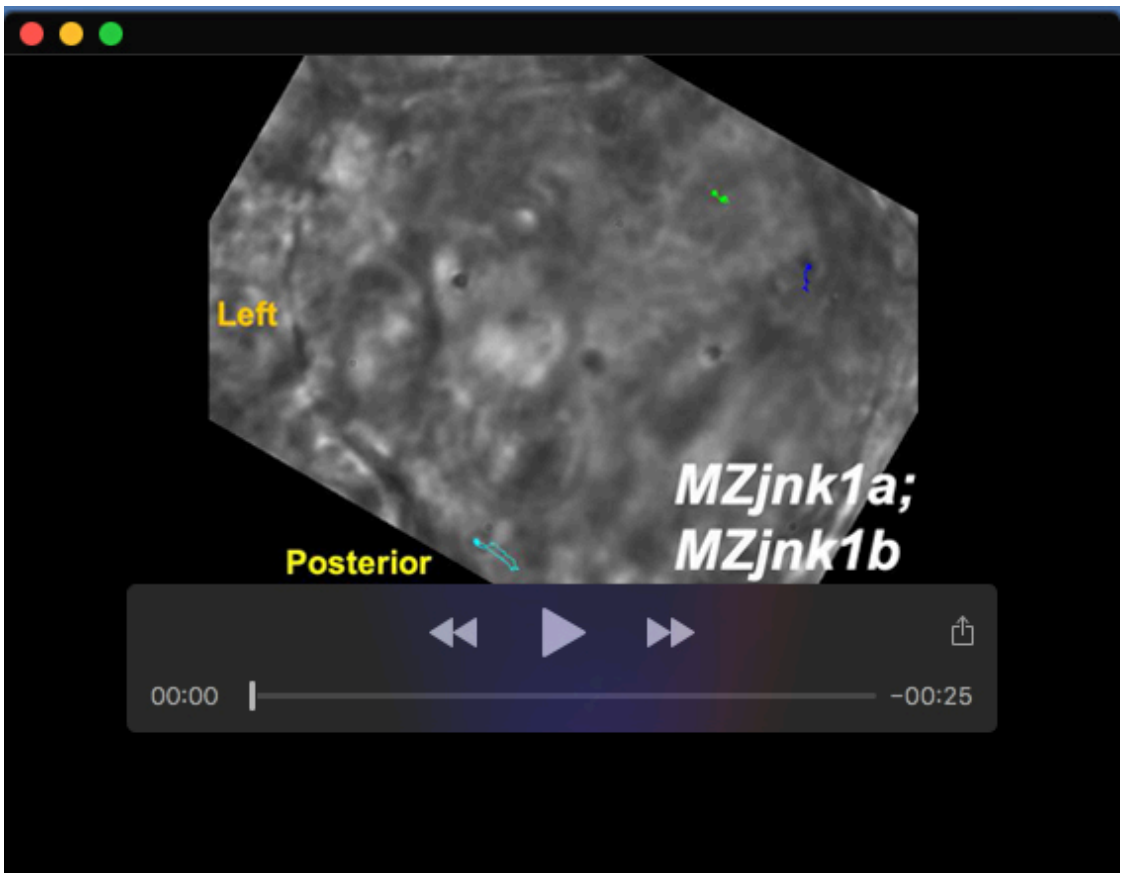

Movie 4. *MZjnk1a;MZjnk1b* Kupffer's Vesicle

Brightfield movie of example *MZjnk1a;MZjnk1b* Kupffer's vesicle injected with beads for quantification of nodal flow, imaged using a 60X objective. Dark blue and green traces: Representative Anterior, red and light blue traces: Representative Posterior.

Movie 5. *MZjnk2* Kupffer's Vesicle

Brightfield movie of example *MZjnk2* Kupffer's vesicle injected with beads for quantification of nodal flow, imaged using a 60X objective. Dark blue and green traces: Representative Anterior, red and light blue traces: Representative Posterior.

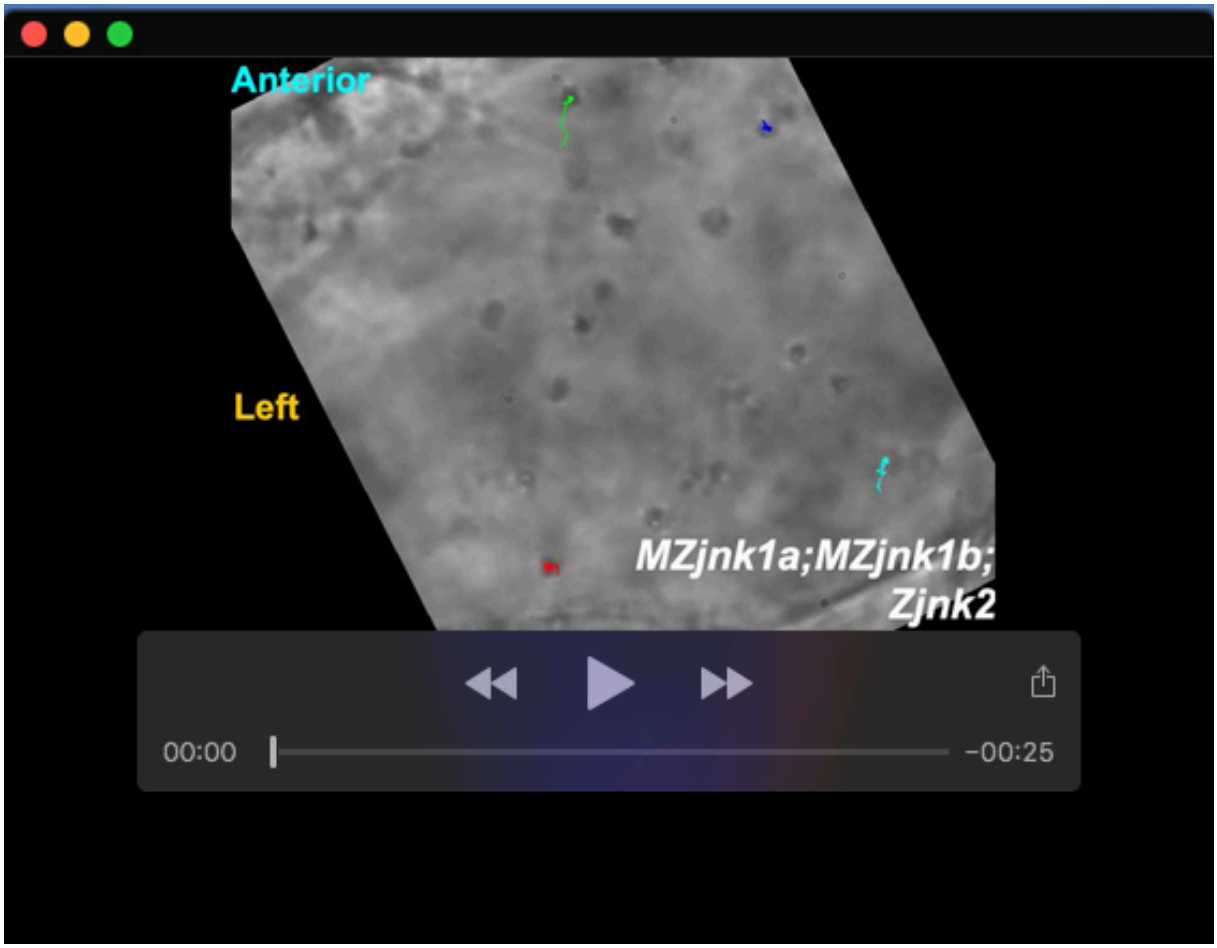

Movie 6. *MZjnk1a;MZjnk1b;Zjnk2* Kupffer's Vesicle

Brightfield movie of example *MZjnk1a;MZjnk1b;Zjnk2* Kupffer's vesicle injected with beads for quantification of nodal flow, imaged using a 60X objective. Nodal flow is dramatically reduced, with beads showing very little directional movement. Dark blue and green traces: Representative Anterior, red and light blue traces: Representative Posterior.

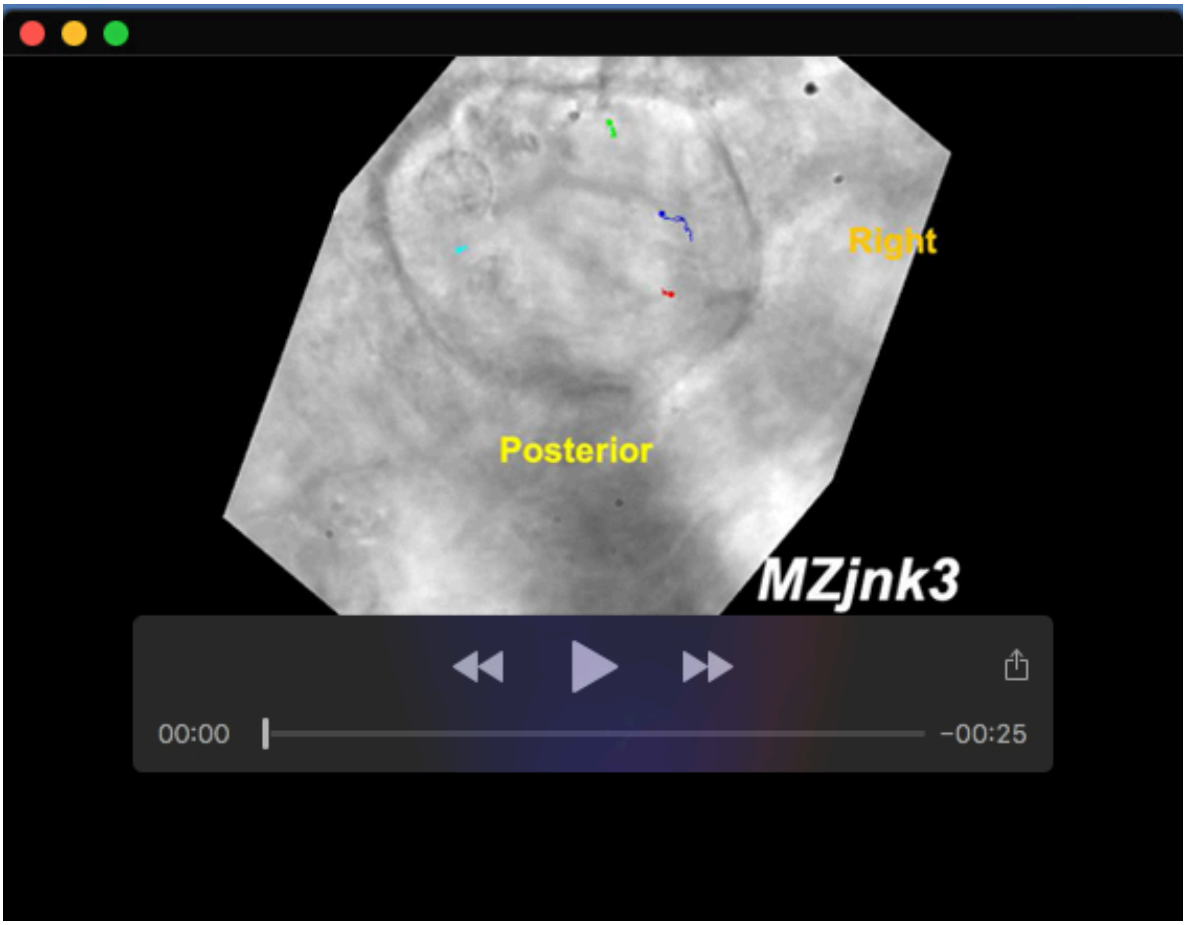

Movie 7. *MZjnk3* Kupffer's Vesicle

Brightfield movie of example *MZjnk3* Kupffer's vesicle injected with beads for quantification of nodal flow, imaged using a 40X objective. Dark blue and green traces: Representative Anterior, red and light blue traces: Representative Posterior.

Movie 8. *MZjnk1a;MZjnk1b;Zjnk3* Kupffer's Vesicle

Brightfield movie of example *MZjnk1a;MZjnk1b;Zjnk3* Kupffer's vesicle injected with beads for quantification of nodal flow, imaged using a 40X objective. Dark blue and green traces: Representative Anterior, red and light blue traces: Representative Posterior.